



HAL
open science

Optimal, Recursive and Suboptimal Linear Solutions to Attitude Determination from Vector Observations

Zebo Zhou, Jin Wu, Jinling Wang, Hassen Fourati

► **To cite this version:**

Zebo Zhou, Jin Wu, Jinling Wang, Hassen Fourati. Optimal, Recursive and Suboptimal Linear Solutions to Attitude Determination from Vector Observations. 2017. hal-01525603v4

HAL Id: hal-01525603

<https://inria.hal.science/hal-01525603v4>

Preprint submitted on 11 Dec 2017

HAL is a multi-disciplinary open access archive for the deposit and dissemination of scientific research documents, whether they are published or not. The documents may come from teaching and research institutions in France or abroad, or from public or private research centers.

L'archive ouverte pluridisciplinaire **HAL**, est destinée au dépôt et à la diffusion de documents scientifiques de niveau recherche, publiés ou non, émanant des établissements d'enseignement et de recherche français ou étrangers, des laboratoires publics ou privés.



Distributed under a Creative Commons Attribution 4.0 International License

Article

Optimal, Recursive and Sub-optimal Linear Solutions to Attitude Determination from Vector Observations for GNSS/Accelerometer/Magnetometer Orientation Measurement

Zebo Zhou ^{1,†} , Jin Wu ^{1,2,†}, Jinling Wang ³, Hassen Fourati ⁴

¹ School of Aeronautics and Astronautics, University of Electronic Science and Technology of China, Chengdu, China; klinsmann.zhou@gmail.com

² School of Automation, University of Electronic Science and Technology of China, Chengdu, China; jin_wu_uestc@hotmail.com

³ University of New South Wales, New South Wales, Australia; Jinling.Wang@unsw.edu.au

⁴ University Grenoble Alpes, CNRS, GIPSA-Lab, Grenoble 38400, France; hassen.fourati@gipsa-lab.grenoble-inp.fr

* Correspondence: jin_wu_uestc@hotmail.com; klinsmann.zhou@gmail.com, Tel.: +86-18615745916

† Zebo Zhou and Jin Wu contributed equally on the theory and experiment of this paper.

‡ The MATLAB source codes of the proposed algorithms are uploaded as open-source files on <https://github.com/zarathustr/OLEQs>.

Academic Editor: name

Version December 11, 2017 submitted to Remote Sens.

Abstract: Integration of accelerometer and magnetometer (AM) provides continuous, stable and accurate attitude information for land-vehicle navigation campaigns. However, magnetic disturbance strongly degrades the overall system performance. As an important complementary, global navigation satellite system (GNSS) indirectly produces the orientation information thus can potentially benefit the AM system. Such GNSS/AM system for attitude estimation is mathematically converted to multi-observation vector pairs matching problem in this paper. The optimal, sub-optimal attitude determination and its time-varying recursive variants are all comprehensively investigated and discussed. The developed methods are named as the Optimal Linear Estimator of Quaternion (OLEQ), Suboptimal-OLEQ (SOLEQ) and Recursive-OLEQ (ROLEQ) for different application scenarios. The theory is established based on our previous contributions and the multi-vector matrix multiplications are decomposed with the eigenvalue factorization. Some analytical results are proved and given which provides the audience with a brand new viewpoint of the attitude determination and its evolution inside. With the derivations of two-vector case, the n -vector case is then naturally formed. Simulations are carried out showing the advantages of accuracy, robustness and time consumption of the proposed OLEQs, compared with representative methods. The algorithms are then implemented using C++ programming language on the designed hardware with GNSS module, 3-axis accelerometer, 3-axis magnetometer, giving the effectiveness validation of them in real-world applications.

Keywords: Attitude Determination, GNSS Receiver, Wahba's Problem, Vector Observations, Autonomous Navigation

0. Introduction

Attitude determination (or estimation) from vector observation pairs is a significant technology in aerospace engineering and related geodetic applications [1–3]. For instance, the inertial navigation, as

an important role in modern military applications, has a high demand on attitude determination accuracy for initial alignment [4–7]. A typical attitude measuring system integrating 3-axis accelerometer with 3-axis magnetometer (AM) is extensively applied for real-time, continuous, stable and accurate attitude estimation for various navigation campaigns [8,9]. For most of applications, AM sensors are very efficient for low-cost attitude determination. However, the magnetometer is easily to be tolerated by unknown and unexpected magnetic fields disturbances from electromagnetic signals contaminated environments. On the other hand, for the large-scale region application, the reference magnetic vector is no longer a constant vector and needs to be timely corrected by other additional heading information. Otherwise, the overall system performance will be heavily degraded. Moreover, the accelerometers inevitably suffer from their biases thus leading to inaccurate attitude estimation. Therefore, auxiliary sensors are necessary to overcome such problem.

Alternatively, the global navigation satellite system (GNSS) provides precise position and velocity information. It has been successfully used for land, marine and aircraft attitude determination applications [10]. Traditional methods integrate GNSS with inertial sensors and simultaneously estimate the orientation with a synchronized position, velocity and attitude loops [11–13]. However, this leads to a risk to contaminate the attitude solution associated with position and velocity estimation loops. Thus Gebre-Egziabher and Elkaim [14] proposes an independent attitude estimation loop by means of vector matching. Compared with GNSS antenna arrays which compute highly precise solutions of baselines by using carrier-phase measurement, single GNSS antenna is more preferred in many low-cost and low-power consumption platforms. It mainly uses the simultaneous velocity vector information generated by GNSS Doppler [15,16]. Indirectly, this produces an important complementary orientation information thus potentially benefits the AM sensors system, especially for land vehicles. In addition, integrating high-rate sensors also contributes to seismogeodetic systems [17,18].

Efficient attitude estimation strategy is very crucial for GNSS/AM integrated multi-sensor system. In essence, it can be mathematically converted to multi-observation vector pairs matching problem. Representative methods are mainly about the solutions to the famous Wahba's problem [19], which aims to obtain the optimal attitude determination results using weighted least squares. Among these algorithms, the Shuster's QUaternion ESTimator (QUEST, [20]), Markley's Singular Value Decomposition (SVD, [21]) and Mortari's (ESOQ, [22]) are the most frequently used ones, which are mostly inspired by Davenport's q-method [23,24]. Our newly developed Fast Linear Attitude Estimator (FLAE, [25]) obtains a fastest Wahba's solution to our existing knowledge. Some other interesting approaches are proposed as well, investigating the other internals of this problem e.g. Yang's analytical method, Riemannian-manifold algorithm and Forbes' Linear-Matrix-Inequality (LMI) solution. [26–28].

There are still some weight-less algorithms for multi-sensor attitude determination. They are usually used on applications like vision attitude determination where the a priori information of weights can hardly be accurately determined. For example, using the nonlinear special orthogonal group on SO3 [29], it is able to obtain the attitude quaternion from arbitrary pairs of vectors. Via optimization approaches like gradient-decent algorithm (GDA, [30]), Gauss-Newton algorithm (GNA, [9]), we may also compute stable solutions. Apart from these, a famous analytical method was proposed by Arun et al. where the Singular Value Decomposition (SVD) is employed to calculate the attitude matrix [31]. Invoking similar commitment, it is then introduced in computing both the attitude and translation vector in machine vision systems [32].

For Wahba's problem, it has been shown that most existing algorithms are based on the Davenport's q-method. For a long period, the attitude solving process is fixed on this framework which aims to find the largest eigenvalue of the Davenport matrix \mathbf{K} . Is it possible to seek another quite different attitude determination approach? The answer is positive and in this paper, three novel quaternion attitude determination algorithms from pairs of vector measurements are proposed in the sense of optimal, time-recursive and sub-optimal formulations. The main contributions are listed below:

- 74 1. The main theory is based on our previous research contributions and is extended to arbitrary
 75 pairs vector measurements linearly for GNSS/AM attitude application.
 76 2. Three estimators i.e. the Optimal Linear Estimator of Quaternion (OLEQ), Recursive OLEQ
 77 (ROLEQ) and Sub-optimal OLEQ (SOLEQ) are derived. We also proposed accelerating techniques
 78 to make the algorithms faster.
 79 3. Simulations and real experiments are carried out, which verify the accuracy, flexibility, robustness
 80 and time consumption of various algorithms for GNSS/AM attitude determination. Detailed
 81 comparisons with representative methods are shown to draw the superiority of the proposed
 82 OLEQs.

83 This paper is structured as follows: Section I briefs the GNSS-AM sensor system along with
 84 its functional and stochastic models formulated in the way of vector pair matching. Section II
 85 contains the problem formulation and starts with the quaternion estimation from a single sensor
 86 observation. Section III The two-vector attitude determination theory along with the n -vector one are
 87 given accordingly. Section IV involves the numerical examples and real field test where comparisons
 88 between the proposed SOLEQ and other representative methods are given. Finally, Section V consists
 89 of concluding remarks and future work.

90 1. Fundamentals of GNSS/AM system

For attitude determination, we require GNSS receivers and AM sensors arrays for low-cost and accurate solutions. First, considering the motion behaviours of land vehicles, a vector pair for GNSS velocity can be established as

$$\mathbf{v}_G^b = \mathbf{C}_r^b \mathbf{v}_G^r + \varepsilon_G^b \quad (1)$$

where \mathbf{v} denotes velocity vector; the subscript G denotes the observation source 'GNSS'; the symbol r and b represent the navigation frame (r -frame, North-East-Down, NED) and body frame (b -frame, Forward-Right-Down) respectively; transforms the vector from r -frame to b -frame; ε_G^b is the Gaussian white noise with variance of \mathbf{R}_G . For land-vehicle application, it should be pointed out that the velocity in r -frame and b -frame are respectively

$$\mathbf{v}^r = \mathbf{C}_e^r \mathbf{v}^e, \mathbf{v}_G^e = \begin{bmatrix} \sqrt{(v_x^e)^2 + (v_y^e)^2 + (v_z^e)^2} \\ 0 \\ 0 \end{bmatrix} \quad (2)$$

where e denotes an Earth-Centred-Earth-Fixed (ECEF) coordinate frame (e -frame), i.e. WGS-84; denotes the transformation (from e -frame to n -frame) and can be computed according to the GNSS position and Earth ellipsoid metrics in advance.

AM sensors consist of 3-axis MEMS accelerometer and 3-axis magnetometer. The accelerometer gives the specific force measurement of a rigid body and magnetometer provides the users with sensed local Earth geomagnetic field according to IGRF model.

$$\begin{aligned} \mathbf{z}_A &= \mathbf{C}_r^b (\boldsymbol{\mu}^r - \mathbf{G}^r) + \mathbf{b}_A + \varepsilon_A, & \varepsilon_A &\sim (\mathbf{0}, \mathbf{R}_A) \\ \mathbf{z}_M &= \mathbf{C}_r^b \mathbf{M}^r + \varepsilon_M, & \varepsilon_M &\sim (\mathbf{0}, \mathbf{R}_M) \end{aligned} \quad (3)$$

where the subscripts A and M denote the accelerometer and magnetometer sources respectively; \mathbf{z} denotes observed vector; \mathbf{b} denotes the accelerometer bias; $\mathbf{G}^r = [0, 0, -g]^T$ where g the gravity, is a function of geo-location; The normalized Earth's magnetic field reference vector $\mathbf{M}^r = [\cos\alpha, 0, -\sin\alpha]^T$ where α is the local dip angle; $\boldsymbol{\mu}$ is the linear acceleration vector which is usually treated as an external disturbance; ε is the Gaussian white noise with the variance of \mathbf{R} . For simplicity, two points need to be clarified that: (1) the bias term has been obtained and compensated for the accelerometer readings. (2) The linear acceleration $\boldsymbol{\mu}$ is estimated by using GNSS velocity information with differentiation between

two adjacent epochs. Then the the vectors and matrices for system model in b -frame and r -frame can be merged into following multi-vector pair equations:

$$\mathbf{D}_i^b = \mathbf{C}_r^b \mathbf{D}_i^r + \varepsilon_i, i = 1, 2, 3 \quad (4)$$

where

$$\begin{pmatrix} \mathbf{D}_1^b \\ \mathbf{D}_2^b \\ \mathbf{D}_3^b \end{pmatrix} = \begin{pmatrix} \frac{\mathbf{v}_G^b}{\|\mathbf{v}_G^b\|} \\ \frac{\mathbf{z}_A}{\|\mathbf{z}_A\|} \\ \frac{\mathbf{z}_M}{\|\mathbf{z}_M\|} \end{pmatrix}, \begin{pmatrix} \mathbf{D}_1^r \\ \mathbf{D}_2^r \\ \mathbf{D}_3^r \end{pmatrix} = \begin{pmatrix} \frac{\mathbf{C}_e^r \mathbf{v}^e}{\|\mathbf{C}_e^r \mathbf{v}^e\|} \\ \frac{\boldsymbol{\mu}^r - \mathbf{G}^r}{\|\boldsymbol{\mu}^r - \mathbf{G}^r\|} \\ \frac{\mathbf{M}^r}{\|\mathbf{M}^r\|} \end{pmatrix}, \begin{pmatrix} \varepsilon_1 \\ \varepsilon_2 \\ \varepsilon_3 \end{pmatrix} = \begin{pmatrix} \varepsilon_G \\ \varepsilon_A \\ \varepsilon_M \end{pmatrix} \quad (5)$$

Neglecting the cross-correlations between sensors, the stochastic model of system is

$$\begin{pmatrix} \varepsilon_G \\ \varepsilon_A \\ \varepsilon_M \end{pmatrix} \sim (\mathbf{0}, \mathbf{R}), \mathbf{R} = \begin{pmatrix} \mathbf{R}_G & & \\ & \mathbf{R}_A & \\ & & \mathbf{R}_M \end{pmatrix} \quad (6)$$

91 2. Problem Formulation

The conventional Wahba's problem aims to find the optimal attitude matrix from vector observation pairs in the sense of least squares, such that

$$L(\mathbf{C}) = \sum_{i=1}^n a_i \|\mathbf{D}_i^b - \mathbf{C} \mathbf{D}_i^r\|^2, n = 2, 3, \dots \quad (7)$$

in which \mathbf{C} denotes the optimal direction cosine matrix (DCM); $\mathbf{D}_i^b = (D_{x,i}^b, D_{y,i}^b, D_{z,i}^b)^\top$ and $\mathbf{D}_i^r = (D_{x,i}^r, D_{y,i}^r, D_{z,i}^r)^\top$ are the i -th pair of normalized vector observations from the body frame b and the reference frame r respectively; a_i is the weight of the i -th sensor output, which is given by the standard deviations of the input vectors from σ_1 to σ_n :

$$a_i = \frac{\sigma_{tot}^2}{\sigma_i^2}, \sigma_{tot}^2 = \frac{1}{\sum_{i=1}^n \frac{1}{\sigma_i^2}} \quad (8)$$

92 provided that the variance information such as shown in (6) is predetermined. Wahba's problem
 93 is solved via many representative methods [33]. Many of these algorithms solve the problem via
 94 eigenvalue decompositions analytically or numerically [26,27]. When there are only one pair of vector
 95 observations, the Wahba's solutions fail to obtain the optimal quaternion since there will be ambiguous
 96 quaternions corresponding to the maximum eigenvalue 1 [34,35]. In our previous contribution [36],
 97 the continuous stable quaternion solution to an accelerometer-based attitude determination system is
 98 derived.

99 2.1. Quaternion from A Single Sensor Observation

Considering an attitude determination model from a pair of vector observations

$$\mathbf{D}^b = \mathbf{C} \mathbf{D}^r \quad (9)$$

, this section deals with the attitude determination from a single pair of sensor observations. Note that the DCM is decomposed with quaternions $\mathbf{q} = (q_0, q_1, q_2, q_3)^\top$ [36] via:

$$\mathbf{C} = (\mathbf{P}_1 \mathbf{q}, \mathbf{P}_2 \mathbf{q}, \mathbf{P}_3 \mathbf{q}) \quad (10)$$

in which

$$\mathbf{P}_1 = \begin{pmatrix} q_0 & q_1 & -q_2 & -q_3 \\ -q_3 & q_2 & q_1 & -q_0 \\ q_2 & q_3 & q_0 & q_1 \end{pmatrix}, \mathbf{P}_2 = \begin{pmatrix} q_3 & q_2 & q_1 & q_0 \\ q_0 & -q_1 & q_2 & -q_3 \\ -q_1 & -q_0 & q_3 & q_2 \end{pmatrix}, \mathbf{P}_3 = \begin{pmatrix} -q_2 & q_3 & -q_0 & q_1 \\ q_1 & q_0 & q_3 & q_2 \\ q_0 & -q_1 & -q_2 & q_3 \end{pmatrix} \quad (11)$$

In this section, the theory is extended to arbitrary sensor with exactly the similar approach in [36]. Inserting (10) into (9) gives

$$\mathbf{D}^b = (D_x^r \mathbf{P}_1 + D_y^r \mathbf{P}_2 + D_z^r \mathbf{P}_3) \mathbf{q} \quad (12)$$

It has been proved in [36] that

$$\mathbf{P}_1^\top = \mathbf{P}_1^\dagger, \mathbf{P}_2^\top = \mathbf{P}_2^\dagger, \mathbf{P}_3^\top = \mathbf{P}_3^\dagger \quad (13)$$

100 where \dagger stands for the Moore-Penrose pseudo-inverse. In fact, another property can be shown in the
101 following theorem

102 **Theorem 1.** $\mathbf{P}_1 \mathbf{P}_2^\top + \mathbf{P}_2 \mathbf{P}_1^\top = \mathbf{P}_1 \mathbf{P}_3^\top + \mathbf{P}_3 \mathbf{P}_1^\top = \mathbf{P}_2 \mathbf{P}_3^\top + \mathbf{P}_3 \mathbf{P}_2^\top = \mathbf{0}_{3 \times 3}$.

Proof. This can be proved via brute-force calculation:

$$\mathbf{P}_1 \mathbf{P}_2^\top = \begin{pmatrix} 0 & -q_0^1 + q_1^2 + q_2^2 - q_3^2 & 2q_0q_1 + 2q_2q_3 \\ q_0^1 - q_1^2 - q_2^2 + q_3^2 & 0 & 2q_0q_2 - 2q_1q_3 \\ -2q_0q_1 - 2q_2q_3 & -2q_0q_2 + 2q_1q_3 & 0 \end{pmatrix} \quad (14a)$$

$$\mathbf{P}_2 \mathbf{P}_1^\top = \begin{pmatrix} 0 & q_0^1 - q_1^2 - q_2^2 + q_3^2 & -2q_0q_1 - 2q_2q_3 \\ -q_0^1 + q_1^2 + q_2^2 - q_3^2 & 0 & -2q_0q_2 + 2q_1q_3 \\ 2q_0q_1 + 2q_2q_3 & 2q_0q_2 - 2q_1q_3 & 0 \end{pmatrix}$$

$$\mathbf{P}_1 \mathbf{P}_3^\top = \begin{pmatrix} 0 & 2q_0q_1 - 2q_2q_3 & q_0^1 - q_1^2 + q_2^2 - q_3^2 \\ -2q_0q_1 + 2q_2q_3 & 0 & -2q_1q_2 - 2q_0q_3 \\ -q_0^1 + q_1^2 - q_2^2 + q_3^2 & 2q_1q_2 + 2q_0q_3 & 0 \end{pmatrix} \quad (14b)$$

$$\mathbf{P}_3 \mathbf{P}_1^\top = \begin{pmatrix} 0 & -2q_0q_1 + 2q_2q_3 & -q_0^1 + q_1^2 - q_2^2 + q_3^2 \\ 2q_0q_1 - 2q_2q_3 & 0 & 2q_1q_2 + 2q_0q_3 \\ q_0^1 - q_1^2 + q_2^2 - q_3^2 & -2q_1q_2 - 2q_0q_3 & 0 \end{pmatrix}$$

$$\mathbf{P}_2 \mathbf{P}_3^\top = \begin{pmatrix} 0 & 2q_0q_2 + 2q_1q_3 & -2q_1q_2 + 2q_0q_3 \\ -2q_0q_2 - 2q_1q_3 & 0 & q_0^1 + q_1^2 - q_2^2 - q_3^2 \\ 2q_1q_2 - 2q_0q_3 & -q_0^1 - q_1^2 + q_2^2 + q_3^2 & 0 \end{pmatrix} \quad (14c)$$

$$\mathbf{P}_3 \mathbf{P}_2^\top = \begin{pmatrix} 0 & -2q_0q_2 - 2q_1q_3 & 2q_1q_2 - 2q_0q_3 \\ 2q_0q_2 + 2q_1q_3 & 0 & -q_0^1 - q_1^2 + q_2^2 + q_3^2 \\ -2q_1q_2 + 2q_0q_3 & q_0^1 + q_1^2 - q_2^2 - q_3^2 & 0 \end{pmatrix}$$

103

104 **Lemma 1.** Let $\mathbf{K}(\mathbf{q}) = (D_x^r \mathbf{P}_1 + D_y^r \mathbf{P}_2 + D_z^r \mathbf{P}_3)$, $\mathbf{K}^\top(\mathbf{q}) = \mathbf{K}^\dagger(\mathbf{q})$.

Proof. We have

$$\begin{aligned}
& \mathbf{K}(\mathbf{q})\mathbf{K}^\top(\mathbf{q}) \\
&= (D_x^r \mathbf{P}_1 + D_y^r \mathbf{P}_2 + D_z^r \mathbf{P}_3)(D_x^r \mathbf{P}_1 + D_y^r \mathbf{P}_2 + D_z^r \mathbf{P}_3)^\top \\
&= (D_x^r)^2 \mathbf{P}_1 \mathbf{P}_1^\top + (D_y^r)^2 \mathbf{P}_2 \mathbf{P}_2^\top + (D_z^r)^2 \mathbf{P}_3 \mathbf{P}_3^\top \\
&\quad + D_x^r D_y^r (\mathbf{P}_1 \mathbf{P}_2^\top + \mathbf{P}_2 \mathbf{P}_1^\top) + D_x^r D_z^r (\mathbf{P}_1 \mathbf{P}_3^\top + \mathbf{P}_3 \mathbf{P}_1^\top) + D_y^r D_z^r (\mathbf{P}_2 \mathbf{P}_3^\top + \mathbf{P}_3 \mathbf{P}_2^\top) \\
&= \left[(D_x^r)^2 + (D_y^r)^2 + (D_z^r)^2 \right] \mathbf{I}_{3 \times 3} \\
&= \mathbf{I}_{3 \times 3}
\end{aligned} \tag{15}$$

105 which gives Lemma 1. ■

Hence (12) can be transformed into

$$\mathbf{D}^b = \mathbf{K}(\mathbf{q})\mathbf{q} \Rightarrow \mathbf{K}^\dagger(\mathbf{q})\mathbf{D}^b = \mathbf{q} \Rightarrow \mathbf{K}^\top(\mathbf{q})\mathbf{D}^b = \mathbf{q} \tag{16}$$

Since $\mathbf{K}(\mathbf{q})$ is in the form of quaternion, $\mathbf{K}^\top(\mathbf{q})\mathbf{D}^b$ can be expanded by

$$\mathbf{K}^\top(\mathbf{q})\mathbf{D}^b = D_x^r \mathbf{P}_1^\top \mathbf{D}^b + D_y^r \mathbf{P}_2^\top \mathbf{D}^b + D_z^r \mathbf{P}_3^\top \mathbf{D}^b \tag{17}$$

Also it can be obtained that

$$\mathbf{P}_1^\top \mathbf{D}^b = \begin{pmatrix} D_x^b q_0 + D_z^b q_2 - D_y^b q_3 \\ D_x^b q_1 + D_y^b q_2 + D_z^b q_3 \\ D_z^b q_0 + D_y^b q_1 - D_x^b q_2 \\ -D_y^b q_0 + D_z^b q_1 - D_x^b q_3 \end{pmatrix} = \begin{pmatrix} D_x^b & 0 & D_z^b & -D_y^b \\ 0 & D_x^b & D_y^b & D_z^b \\ D_z^b & D_y^b & -D_x^b & 0 \\ -D_y^b & D_z^b & 0 & -D_x^b \end{pmatrix} \mathbf{q} = \mathbf{M}_1 \mathbf{q} \tag{18a}$$

$$\mathbf{P}_2^\top \mathbf{D}^b = \begin{pmatrix} D_y^b q_0 - D_z^b q_1 + D_x^b q_3 \\ -D_z^b q_0 - D_y^b q_1 + D_x^b q_2 \\ D_x^b q_1 + D_y^b q_2 + D_z^b q_3 \\ D_x^b q_0 + D_z^b q_2 - D_y^b q_3 \end{pmatrix} = \begin{pmatrix} D_y^b & -D_z^b & 0 & D_x^b \\ -D_z^b & -D_y^b & D_x^b & 0 \\ 0 & D_x^b & D_y^b & D_z^b \\ D_x^b & 0 & D_z^b & -D_y^b \end{pmatrix} \mathbf{q} = \mathbf{M}_2 \mathbf{q} \tag{18b}$$

$$\mathbf{P}_3^\top \mathbf{D}^b = \begin{pmatrix} D_z^b q_0 + D_y^b q_1 - D_x^b q_2 \\ D_y^b q_0 - D_z^b q_1 + D_x^b q_3 \\ -D_x^b q_0 - D_z^b q_2 + D_y^b q_3 \\ D_x^b q_1 + D_y^b q_2 + D_z^b q_3 \end{pmatrix} = \begin{pmatrix} D_z^b & D_y^b & -D_x^b & 0 \\ D_y^b & -D_z^b & 0 & D_x^b \\ -D_x^b & 0 & -D_z^b & D_y^b \\ 0 & D_x^b & D_y^b & D_z^b \end{pmatrix} \mathbf{q} = \mathbf{M}_3 \mathbf{q} \tag{18c}$$

Then we have

$$\mathbf{K}^\top(\mathbf{q})\mathbf{D}^b = D_x^r \mathbf{M}_1 \mathbf{q} + D_y^r \mathbf{M}_2 \mathbf{q} + D_z^r \mathbf{M}_3 \mathbf{q} = \mathbf{W} \mathbf{q} \tag{19}$$

where \mathbf{W} is given by

$$\mathbf{W} = D_x^r \mathbf{M}_1 + D_y^r \mathbf{M}_2 + D_z^r \mathbf{M}_3 \tag{20}$$

Therefore the attitude determination problem is shifted to

$$\mathbf{W} \mathbf{q} = \mathbf{q} \tag{21}$$

106 **Theorem 2.** For any normalized vector observation pair $\{\mathbf{D}^r, \mathbf{D}^b\}$, $\mathbf{W}^2 = \mathbf{I}$, where \mathbf{I} is the four-order identity
107 matrix.

Proof. The characteristic polynomial of \mathbf{W} is given by

$$p(\lambda) = (\lambda - 1)^2 (\lambda + 1)^2 \tag{22}$$

Then with Cayley-Hamilton Theorem, we substitute \mathbf{W} for its eigenvalues and obtain

$$\left(\mathbf{W}^2 - \mathbf{I}\right)^2 = \mathbf{0} \quad (23)$$

108 as $\mathbf{W}^2 - \mathbf{I}$ is real symmetric, it should be $\mathbf{0}$, which finishes the proof. \blacksquare

In [36], we showed that (21) can be seen as an iterative dynamical system

$$\mathbf{q}(n) = \mathbf{W}\mathbf{q}(n-1) \quad (24)$$

where $\mathbf{q}(n)$ denotes the quaternion for the n th iteration. Also, as has been proved, the discrete system can be converted to a corresponding continuous system. The stable solution to the continuous system is calculated as

$$\mathbf{q} = \frac{\mathbf{W} + \mathbf{I}}{2} \mathbf{q}_{rand} \quad (25)$$

109 if $\mathbf{W}^2 = \mathbf{I}$. Where \mathbf{q}_{rand} denotes an randomly-chosen unit quaternion. This provides us with a new
110 approach to obtaining the measurement quaternion from a single strapdown sensor.

111 3. Optimal Linear Estimator of Quaternion

With (9), it is able to list all the single rotation equations together as follows:

$$\begin{cases} \mathbf{D}_1^b = \mathbf{C}\mathbf{D}_1^r \\ \mathbf{D}_2^b = \mathbf{C}\mathbf{D}_2^r \\ \vdots \\ \mathbf{D}_n^b = \mathbf{C}\mathbf{D}_n^r \end{cases} \Rightarrow \begin{cases} \sqrt{a_1}\mathbf{D}_1^b = \sqrt{a_1}\mathbf{C}\mathbf{D}_1^r \\ \sqrt{a_2}\mathbf{D}_2^b = \sqrt{a_2}\mathbf{C}\mathbf{D}_2^r \\ \vdots \\ \sqrt{a_n}\mathbf{D}_n^b = \sqrt{a_n}\mathbf{C}\mathbf{D}_n^r \end{cases} \quad (26)$$

which can in turn be converted to

$$\begin{cases} \sqrt{a_1}\mathbf{q} = \sqrt{a_1}\mathbf{W}_1\mathbf{q} \\ \sqrt{a_2}\mathbf{q} = \sqrt{a_2}\mathbf{W}_2\mathbf{q} \\ \vdots \\ \sqrt{a_n}\mathbf{q} = \sqrt{a_n}\mathbf{W}_n\mathbf{q} \end{cases} \quad (27)$$

This system is rewritten as

$$\begin{pmatrix} \sqrt{a_1}\mathbf{I} \\ \sqrt{a_2}\mathbf{I} \\ \vdots \\ \sqrt{a_n}\mathbf{I} \end{pmatrix} \mathbf{q} = \begin{pmatrix} \sqrt{a_1}\mathbf{W}_1 \\ \sqrt{a_2}\mathbf{W}_2 \\ \vdots \\ \sqrt{a_n}\mathbf{W}_n \end{pmatrix} \mathbf{q} \quad (28)$$

Notice that

$$\left(\sqrt{a_1}\mathbf{I}, \sqrt{a_2}\mathbf{I}, \dots, \sqrt{a_n}\mathbf{I}\right) \begin{pmatrix} \sqrt{a_1}\mathbf{I} \\ \sqrt{a_2}\mathbf{I} \\ \vdots \\ \sqrt{a_n}\mathbf{I} \end{pmatrix} = \left(\sum_{i=1}^n a_i\right) \mathbf{I} = \mathbf{I} \quad (29)$$

Hence the pre-multiplication leads to

$$\mathbf{q} = \left(\sum_{i=1}^n a_i \mathbf{W}_i\right) \mathbf{q} \quad (30)$$

It should be then noted that (28) is free of the existence of noises. In fact, the optimal attitude determination i.e. the Wahba's problem, has been proved as a total least-square problem in which both the reference and observation models are corrupted by the stochastic items. In this case, the maximum eigenvalue of $\sum_{i=1}^n a_i \mathbf{W}_i$ in engineering practice is very close to the noise-free theoretical result of 1. Corresponding with (24), based on the Brouwer's fixed-point theorem, it is able to iteratively obtain the normalized optimal quaternion by rotating a randomly given initial quaternion over and over again till infinity. This is something similar with the power method of the numerical eigenvalue factorization but can be accelerated with geometric-series-like iterations as follows

$$\begin{aligned}\mathcal{R} &= \left(\sum_{i=1}^n a_i \mathbf{W}_i \right) \\ \mathcal{R}^2 &= \mathcal{R} \cdot \mathcal{R} \\ &\vdots \\ \mathcal{R}^{2^j} &= \mathcal{R}^{2^{j-1}} \cdot \mathcal{R}^{2^{j-1}}\end{aligned}\quad (31)$$

where \mathcal{R} denotes the rotation operator over the Hamilton space \mathbb{H} . In fact, the above iterations can hardly be achieved when the maximum eigenvalue approaches 1. The reason is that at this time the power \mathcal{R}^2 approaches \mathbf{I} as well. A more robust way is shown to solve this problem. Considering the both sides of (28), we may find out that the right side is in fact the mixture of solutions to single vector observation pairs. As mentioned in (25), a stable, continuous solution to each single equation can be done by pre-multiplying $\frac{1}{2}(\mathbf{W}_i + \mathbf{I})$. Substituting $\frac{1}{2}(\mathbf{W}_i + \mathbf{I})$ for \mathbf{W}_i , i.e.

$$\begin{pmatrix} \sqrt{a_1} \mathbf{I} \\ \sqrt{a_2} \mathbf{I} \\ \vdots \\ \sqrt{a_n} \mathbf{I} \end{pmatrix} \mathbf{q} = \begin{bmatrix} \frac{1}{2} \sqrt{a_1} (\mathbf{W}_1 + \mathbf{I}) \\ \frac{1}{2} \sqrt{a_2} (\mathbf{W}_2 + \mathbf{I}) \\ \vdots \\ \frac{1}{2} \sqrt{a_n} (\mathbf{W}_n + \mathbf{I}) \end{bmatrix} \mathbf{q} \quad (32)$$

, the quaternion evolutes from the mixture of single optimal solution. Here, the rotation operator is revised as

$$\mathcal{R} = \sum_{i=1}^n \frac{1}{2} a_i (\mathbf{W}_i + \mathbf{I}) = \frac{1}{2} \left(\mathbf{I} + \sum_{i=1}^n a_i \mathbf{W}_i \right) \quad (33)$$

This equals to the least-square of the set of pre-computed single rotated quaternion, which is definitely faster and more robust than rotation from a randomly given initial quaternion.

The covariance of the calculated optimal quaternion is equal to that of QUEST under the condition of least-square optimality:

$$\begin{aligned}\Sigma_{\mathbf{Q},\text{OLEQ}} &= \frac{1}{4} \sigma_{tot}^2 \left(\mathbf{I} - \sum_{i=1}^n \mathbf{D}^b \{ \mathbf{D}^b \}^\top \right) \\ \Sigma_{\mathbf{q},\text{OLEQ}} &= [\mathbf{q}_{opt}] \begin{pmatrix} 0 & \mathbf{0}_{1 \times 3} \\ \mathbf{0}_{3 \times 1} & \Sigma_{\mathbf{Q},\text{OLEQ}} \end{pmatrix} [\mathbf{q}_{opt}]^\top\end{aligned}\quad (34)$$

where $\mathbf{Q} = (q_1, q_2, q_3)^\top$ is the vector part of the quaternion. $[\mathbf{q}]$ defines the following matrix

$$[\mathbf{q}] = \begin{pmatrix} q_3 & -q_2 & q_1 & q_0 \\ q_2 & q_3 & -q_0 & q_1 \\ -q_1 & q_0 & q_3 & q_2 \\ -q_0 & -q_1 & -q_2 & q_3 \end{pmatrix} \quad (35)$$

112 3.1. Variant One: Recursive-OLEQ

We have seen from the above formulations that for each epoch, the vector observations are batchedly processed thoroughly. When used in aerospace electronic systems, the measured vector observation pairs in neighboring time epochs are usually continuous since they are always been smoothed by the sum filters and low-pass filters (LPF). Therefore, with this consideration, the attitude quaternion can be propagated from the last estimated one using the rotation operator described before. In this way the quaternions are recursively computed with much less computations and the accuracy is maintained. A more convenient clue is that for high reliable attitude determination systems, high-precision rate gyroscopes are employed usually. This provides us with a second-stage accelerating scheme, inspired by the conventional recursive algorithms like filter QUEST, REQUEST and etc. [37], that we may first rotate the estimated quaternion in last time epoch with zero-order angular transition matrix by

$$\mathbf{q}_k = \Phi_{k,k-1} \mathbf{q}_{k-1} \quad (36)$$

where

$$\Phi_{k,k-1} = \mathbf{I} + \frac{\Delta t}{2} [\mathbf{\Omega} \times] \quad (37)$$

in which Δt is the sampling time and $[\mathbf{\Omega} \times]$ composed by the angular rate from the gyroscope, which is detailed in many classical literatures. After this, even a single rotation by \mathcal{R} would be very accurate then. The one-step covariance matrix of the obtained quaternion is calculated by

$$\Sigma_{\mathbf{q}_k, \text{ROLEQ}} = \mathcal{R} \Phi_{k,k-1} \Sigma_{\mathbf{q}_{k-1}, \text{ROLEQ}} \Phi_{k,k-1}^\top \mathcal{R}^\top \quad (38)$$

113 3.2. Variant Two: SOLEQ

114 3.2.1. Two-Vector Case

When there are two pairs of vector observations, regardless of the weights of respective sensors, it is natural that the attitude quaternion may be computed via

$$\mathbf{q} = \frac{1}{4} (\mathbf{W}_1 + \mathbf{I}) (\mathbf{W}_2 + \mathbf{I}) \mathbf{q}_{rand} \quad (39)$$

where \mathbf{W}_1 and \mathbf{W}_2 are for the 1st and 2nd sensors. (25) is reasonable since we have

$$\left[\frac{1}{2} (\mathbf{W} + \mathbf{I}) \right]^2 = \frac{1}{4} (\mathbf{W}^2 + 2\mathbf{W} + \mathbf{I}) = \frac{1}{4} (2\mathbf{W} + 2\mathbf{I}) = \frac{1}{2} (\mathbf{W} + \mathbf{I}) \quad (40)$$

However, for the two-vector case, one can write

$$\left[\frac{1}{4} (\mathbf{W}_1 + \mathbf{I}) (\mathbf{W}_2 + \mathbf{I}) \right]^2 = \left[\frac{1}{4} (\mathbf{W}_1 \mathbf{W}_2 + \mathbf{W}_1 + \mathbf{W}_2 + \mathbf{I}) \right]^2 \neq \frac{1}{4} (\mathbf{W}_1 + \mathbf{I}) (\mathbf{W}_2 + \mathbf{I}) \quad (41)$$

This reflects that the accurate quaternion may be recursively computed with

$$\begin{cases} \mathbf{q}_k = \frac{1}{4} (\mathbf{W}_1 + \mathbf{I}) (\mathbf{W}_2 + \mathbf{I}) \mathbf{q}_{k-1} \\ \mathbf{q}_k = \frac{\mathbf{q}_k}{\|\mathbf{q}_k\|} \end{cases} \quad (42)$$

which exits when the Euler distance $\|\mathbf{q}_k - \mathbf{q}_{k-1}\|$ is less than one predetermined threshold η . Note that the above initialization procedure is equivalent to the following process

$$\begin{cases} \mathbf{q}^j = \left[\frac{1}{4} (\mathbf{W}_1 + \mathbf{I}) (\mathbf{W}_2 + \mathbf{I}) \right]^j \mathbf{q}_{rand} \\ \mathbf{q}^j = \frac{\mathbf{q}^j}{\|\mathbf{q}^j\|} \end{cases} \quad (43)$$

where j is chosen to make sure $\|\mathbf{q}^j - \mathbf{q}^{j-1}\| < \eta$. Let us define some notations i.e. transformation operators

$$\mathcal{A} = \frac{1}{4} (\mathbf{W}_1 + \mathbf{I}) (\mathbf{W}_2 + \mathbf{I}) \quad (44a)$$

$$\mathcal{B} = \mathcal{A}^\top = \frac{1}{4} (\mathbf{W}_2 + \mathbf{I}) (\mathbf{W}_1 + \mathbf{I}) \quad (44b)$$

Theorem 3. For the two-vector attitude determination case, the steady-state evolution in (43) is not affected by transformation operators' order, such that

$$\begin{cases} \mathbf{q}^j = \mathcal{A}^j \mathbf{q}_{rand} \\ \mathbf{q}^j = \frac{\mathbf{q}^j}{\|\mathbf{q}^j\|} \end{cases} \Leftrightarrow \begin{cases} \mathbf{q}^j = \mathcal{B}^j \mathbf{q}_{rand} \\ \mathbf{q}^j = \frac{\mathbf{q}^j}{\|\mathbf{q}^j\|} \end{cases}, j \rightarrow +\infty \quad (45)$$

Proof. The integrated transformation can be computed by

$$\begin{aligned} \mathcal{A}\mathcal{B} &= \frac{1}{16} (\mathbf{W}_1 + \mathbf{I}) (\mathbf{W}_2 + \mathbf{I})^2 (\mathbf{W}_1 + \mathbf{I}) = \frac{1}{8} (\mathbf{W}_1 + \mathbf{I}) (\mathbf{W}_2 + \mathbf{I}) (\mathbf{W}_1 + \mathbf{I}) \\ &= \frac{1}{2} \mathcal{A} (\mathbf{W}_1 + \mathbf{I}) = \frac{1}{2} (\mathbf{W}_1 + \mathbf{I}) \mathcal{B} \end{aligned} \quad (46)$$

and accordingly

$$\mathcal{B}\mathcal{A} = \frac{1}{2} \mathcal{B} (\mathbf{W}_2 + \mathbf{I}) = \frac{1}{2} (\mathbf{W}_2 + \mathbf{I}) \mathcal{A} \quad (47)$$

These generate

$$\mathcal{A}\mathcal{B}\mathcal{A} = \frac{1}{2} (\mathbf{W}_1 + \mathbf{I}) \mathcal{B}\mathcal{A} = \frac{1}{4} (\mathbf{W}_1 + \mathbf{I}) (\mathbf{W}_2 + \mathbf{I}) \mathcal{A} = \mathcal{A}^2 \quad (48)$$

and

$$\mathcal{A}\mathcal{B}\mathcal{A}\mathcal{B} = \mathcal{A}^2\mathcal{B} = \mathcal{A} (\mathcal{A}\mathcal{B}) = \frac{1}{2} \mathcal{A}^2 (\mathbf{W}_1 + \mathbf{I}) \quad (49)$$

Finally, we have

$$(\mathcal{A}\mathcal{B})^j = \frac{1}{2} \mathcal{A}^j (\mathbf{W}_1 + \mathbf{I}) = \frac{1}{2} (\mathbf{W}_1 + \mathbf{I}) \mathcal{B}^j \quad (50)$$

115 This proves that the mixed steady-state transformation $(\mathcal{A}\mathcal{B})^j$ can be achieved by independent
116 transformations from \mathcal{A} or \mathcal{B} , which finishes the proof. ■

Following this theorem, the confronted problem is to compute the power \mathcal{A}^j . In fact, \mathcal{A} is formed by $\frac{1}{2}(\mathbf{W}_1 + \mathbf{I})$ and $\frac{1}{2}(\mathbf{W}_2 + \mathbf{I})$. Their respective eigenvalue decomposition can be given by

$$\begin{cases} \frac{1}{2}(\mathbf{W}_1 + \mathbf{I}) = \mathbf{V}_1 \mathbf{S}_1 \mathbf{V}_1^{-1} = \mathbf{V}_1 \mathbf{S}_1 \mathbf{V}_1^{\top} \\ \frac{1}{2}(\mathbf{W}_2 + \mathbf{I}) = \mathbf{V}_2 \mathbf{S}_2 \mathbf{V}_2^{-1} = \mathbf{V}_2 \mathbf{S}_2 \mathbf{V}_2^{\top} \end{cases} \quad (51)$$

where \mathbf{V} and \mathbf{D} are constituted by eigenvectors and eigenvalues respectively as $(\mathbf{W}_i + \mathbf{I})$ is real symmetric [38]. Since \mathbf{W}_1 and \mathbf{W}_2 are in the same form, the eigenvalue matrices are equal to each other, i.e.

$$\mathbf{S}_1 = \mathbf{S}_2 = \mathbf{S} \quad (52)$$

Then \mathcal{A} can be rewritten as

$$\mathcal{A} = \mathbf{V}_1 \mathbf{S} \mathbf{V}_1^{\top} \mathbf{V}_2 \mathbf{S} \mathbf{V}_2^{\top} \quad (53)$$

Identically, we have

$$\mathcal{B} = \mathbf{V}_2 \mathbf{S} \mathbf{V}_2^{\top} \mathbf{V}_1 \mathbf{S} \mathbf{V}_1^{\top} \quad (54)$$

Combining (53) and (54), it is obtained that

$$\mathcal{A}\mathcal{B} = \mathbf{V}_1 \mathbf{S} \mathbf{V}_1^{\top} \mathbf{V}_2 \mathbf{S} \mathbf{V}_2^{\top} \mathbf{V}_2 \mathbf{S} \mathbf{V}_2^{\top} \mathbf{V}_1 \mathbf{S} \mathbf{V}_1^{\top} \quad (55)$$

Note that

$$\mathbf{V}_1 \mathbf{V}_1^{\top} = \mathbf{V}_1^{\top} \mathbf{V}_1 = \mathbf{V}_2 \mathbf{V}_2^{\top} = \mathbf{V}_2^{\top} \mathbf{V}_2 = \mathbf{I} \quad (56)$$

(55) is simplified as

$$\mathcal{A}\mathcal{B} = \mathbf{V}_1 \mathbf{S} \mathbf{V}_1^{\top} \mathbf{V}_2 \mathbf{S} \mathbf{V}_2^{\top} \mathbf{V}_1 \mathbf{S} \mathbf{V}_1^{\top} \quad (57)$$

Here we define

$$\mathbf{U} = \mathbf{S} \mathbf{V}_1^{\top} \mathbf{V}_2 \mathbf{S}^2 \mathbf{V}_2^{\top} \mathbf{V}_1 \mathbf{S} \quad (58)$$

Actually it is decomposed by

$$\begin{aligned} \mathbf{U} &= \mathbf{H} \mathbf{H}^{\top} \\ \mathbf{H} &= \mathbf{S} \mathbf{V}_1^{\top} \mathbf{V}_2 \mathbf{S} \end{aligned} \quad (59)$$

An interesting fact is that the eigenvalue matrix \mathbf{S} can be analytically calculated and is given by

$$\mathbf{S} = \text{diag}(0, 0, 1, 1) \quad (60)$$

where $\text{diag}(\cdot)$ represents the diagonal matrix. This further yields \mathbf{H} to be a matrix with the form of

$$\mathbf{H} = \begin{pmatrix} 0 & 0 & 0 & 0 \\ 0 & 0 & 0 & 0 \\ 0 & 0 & h_1 & h_2 \\ 0 & 0 & h_3 & h_4 \end{pmatrix} \quad (61)$$

Then \mathbf{U} is computed by

$$\mathbf{U} = \mathbf{H} \mathbf{H}^{\top} = \begin{pmatrix} 0 & 0 & 0 & 0 \\ 0 & 0 & 0 & 0 \\ 0 & 0 & u_1 & u_2 \\ 0 & 0 & u_3 & u_4 \end{pmatrix} = \begin{pmatrix} 0 & 0 & 0 & 0 \\ 0 & 0 & 0 & 0 \\ 0 & 0 & h_1^2 + h_2^2 & h_1 h_3 + h_2 h_4 \\ 0 & 0 & h_1 h_3 + h_2 h_4 & h_3^2 + h_4^2 \end{pmatrix} \quad (62)$$

where $u_2 = u_3$. Using this, we have

$$(\mathcal{A}\mathcal{B})^j = \mathbf{V}_1 \mathbf{U} \mathbf{V}_1^T \mathbf{V}_1 \mathbf{U} \mathbf{V}_1^T \cdots \mathbf{V}_1 \mathbf{U} \mathbf{V}_1^T = \mathbf{V}_1 \mathbf{U}^j \mathbf{V}_1^T \quad (63)$$

\mathbf{U} can be decomposed with eigenvalue decomposition as well, such that

$$\mathbf{U} = \mathbf{V}_U \mathbf{S}_U \mathbf{V}_U^T \quad (64)$$

which can be analytically given by

$$\mathbf{S}_U = \text{diag} \left(0, 0, -\frac{1}{2} \sqrt{\Delta} + \frac{u_1 + u_4}{2}, +\frac{1}{2} \sqrt{\Delta} + \frac{u_1 + u_4}{2} \right)$$

$$\mathbf{V}_U = \begin{pmatrix} 1 & 0 & 0 & 0 \\ 0 & 1 & 0 & 0 \\ 0 & 0 & \frac{-u_1 + u_4 + \sqrt{\Delta}}{2u_2} & \frac{u_1 - u_4 + \sqrt{\Delta}}{2u_2} \\ 0 & 0 & 1 & 1 \end{pmatrix} \quad (65)$$

with

$$\Delta = u_1^2 - 2u_1u_4 + 4u_2^2 + u_4^2 \quad (66)$$

Letting

$$\lambda_{U,1} = -\frac{1}{2} \sqrt{\Delta} + \frac{u_1 + u_4}{2}$$

$$\lambda_{U,2} = +\frac{1}{2} \sqrt{\Delta} + \frac{u_1 + u_4}{2} \quad (67)$$

, \mathbf{U}^j is finally computed by

$$\mathbf{U}^j = \mathbf{V}_U \mathbf{S}^j \mathbf{V}_U^T = \mathbf{V}_U \text{diag}(0, 0, \lambda_{U,1}^j, \lambda_{U,2}^j) \mathbf{V}_U^T \quad (68)$$

Therefore

$$(\mathcal{A}\mathcal{B})^j = \mathbf{V}_1 \mathbf{U}^j \mathbf{V}_1^T = \mathbf{V}_1 \mathbf{V}_U \text{diag}(0, 0, \lambda_{U,1}^j, \lambda_{U,2}^j) \mathbf{V}_U^T \mathbf{V}_1^T \quad (69)$$

Required computation of \mathbf{V}_i is given by

$$\frac{1}{2} (\mathbf{W}_i + \mathbf{I}) = \tilde{\mathbf{V}}_i \mathbf{S} \tilde{\mathbf{V}}_i^{-1} \quad (70)$$

where $\tilde{\mathbf{V}}_i(x, y)$ stands for the element of $\tilde{\mathbf{V}}_i$ in x -th row and y -th column, whose details are given by (71)

$$\begin{aligned} \tilde{\mathbf{V}}_i(1,1) &= +\frac{1}{V_i} (D_{x,i}^b - D_{x,i}^r) (D_{z,i}^b - D_{z,i}^r) \\ \tilde{\mathbf{V}}_i(1,2) &= -\frac{1}{V_i} (D_{x,i}^b - D_{x,i}^r) (D_{y,i}^b - D_{y,i}^r) \\ \tilde{\mathbf{V}}_i(1,3) &= +\frac{1}{V_i} (D_{x,i}^b + D_{x,i}^r) (D_{z,i}^b + D_{z,i}^r) \\ \tilde{\mathbf{V}}_i(1,4) &= -\frac{1}{V_i} (D_{x,i}^b + D_{x,i}^r) (D_{y,i}^b + D_{y,i}^r) \end{aligned} \quad (71a)$$

$$\begin{aligned}
\tilde{\mathbf{V}}_i(2,1) &= +\frac{1}{V_i}(D_{x,i}^b - D_{x,i}^r)(D_{y,i}^b + D_{y,i}^r) \\
\tilde{\mathbf{V}}_i(2,2) &= +\frac{1}{V_i}(D_{x,i}^b - D_{x,i}^r)(D_{z,i}^b + D_{z,i}^r) \\
\tilde{\mathbf{V}}_i(2,3) &= +\frac{1}{V_i}(D_{x,i}^b + D_{x,i}^r)(D_{y,i}^b - D_{y,i}^r) \\
\tilde{\mathbf{V}}_i(2,4) &= +\frac{1}{V_i}(D_{x,i}^b + D_{x,i}^r)(D_{z,i}^b - D_{z,i}^r)
\end{aligned} \tag{71b}$$

$$\begin{aligned}
\tilde{\mathbf{V}}_i(3,1) &= 1 & \tilde{\mathbf{V}}_i(3,2) &= 0 & \tilde{\mathbf{V}}_i(3,3) &= 1 & \tilde{\mathbf{V}}_i(3,4) &= 0 \\
\tilde{\mathbf{V}}_i(4,1) &= 0 & \tilde{\mathbf{V}}_i(4,2) &= 1 & \tilde{\mathbf{V}}_i(4,3) &= 0 & \tilde{\mathbf{V}}_i(4,4) &= 1
\end{aligned} \tag{71c}$$

in which the factor is computed by

$$V_i = (D_{y,i}^b)^2 + (D_{z,i}^b)^2 - (D_{y,i}^r)^2 - (D_{z,i}^r)^2 \tag{72}$$

Related information can also be acquired from [25]. It should be noted that

$$\tilde{\mathbf{V}}_i \tilde{\mathbf{V}}_i^\top \neq \tilde{\mathbf{V}}_i^\top \tilde{\mathbf{V}}_i \neq \mathbf{I} \tag{73}$$

Thus the Gram-Schmidt orthogonalization should be applied to $\tilde{\mathbf{V}}_i$, enabling $\mathbf{V}_i \mathbf{V}_i^\top = \mathbf{V}_i^\top \mathbf{V}_i = \mathbf{I}$ [38]. A typical commitment to achieve this is to compute the QR decomposition [39], such that

$$\mathbf{V}_i \mathbf{R} = \tilde{\mathbf{V}}_i \tag{74}$$

117 where \mathbf{R} denotes an invertible upper triangular matrix. If $\mathbf{q}_{rand} = (1, 0, 0, 0)$, the suboptimal quaternion
 118 is equal to the normalized first column of $(\mathcal{A}\mathcal{B})^j$.

119 3.2.2. *n*-Vector Case

Corresponding to the above notations and derivations, the *n*-vector case's transformation operators are defined by

$$\begin{aligned}
\mathcal{A} &= \mathbf{V}_1 \mathbf{S} \mathbf{V}_1^\top \cdots \mathbf{V}_i \mathbf{S} \mathbf{V}_i^\top \cdots \mathbf{V}_n \mathbf{S} \mathbf{V}_n^\top \\
\mathcal{B} &= \mathbf{V}_n \mathbf{S} \mathbf{V}_n^\top \cdots \mathbf{V}_i \mathbf{S} \mathbf{V}_i^\top \cdots \mathbf{V}_1 \mathbf{S} \mathbf{V}_1^\top
\end{aligned} \tag{75}$$

Defining

$$\mathbf{H} = \mathbf{S} \mathbf{V}_1^\top \left(\prod_{i=2}^{n-1} \mathbf{V}_i \mathbf{S} \mathbf{V}_i^\top \right) \mathbf{V}_n \mathbf{S} = \frac{1}{2^{n-2}} \mathbf{S} \mathbf{V}_1^\top \left[\prod_{i=2}^{n-1} (\mathbf{W}_i + \mathbf{I}) \right] \mathbf{V}_n \mathbf{S} \tag{76}$$

, we have

$$\mathbf{U} = \mathbf{S} \mathbf{V}_1^\top \cdots \mathbf{V}_i \mathbf{S} \mathbf{V}_i^\top \cdots \mathbf{V}_n \mathbf{S}^2 \mathbf{V}_n^\top \cdots \mathbf{V}_i \mathbf{S} \mathbf{V}_i^\top \cdots \mathbf{V}_1 \mathbf{S} = \mathbf{H} \mathbf{H}^\top \tag{77}$$

Then

$$\mathcal{A}\mathcal{B} = \mathbf{V}_1 \mathbf{U} \mathbf{V}_1^\top \Rightarrow (\mathcal{A}\mathcal{B})^j = \mathbf{V}_1 \mathbf{U}^j \mathbf{V}_1^\top = \mathbf{V}_1 \mathbf{V}_U \text{diag}(0, 0, \lambda_{U,1}^j, \lambda_{U,2}^j) \mathbf{V}_U^\top \mathbf{V}_1^\top \tag{78}$$

120 Accordingly, the normalized first column of $(\mathcal{A}\mathcal{B})^j$ constitutes the attitude quaternion.

122 3.2.3. The Effect of Power Order

In this sub-section we show that the selection of j is in fact not influential to the final result at all. Letting

$$\begin{aligned} g_1 &= \frac{-u_1 + u_4 + \sqrt{\Delta}}{2u_2} \\ g_2 &= \frac{u_1 - u_4 + \sqrt{\Delta}}{2u_2} \end{aligned} \quad (79)$$

we have

$$\begin{aligned} (\mathcal{AB})^j(x, y) &= \mathbf{V}_1 \mathbf{V}_U \text{diag}(0, 0, \lambda_{U,1}^j, \lambda_{U,2}^j) \mathbf{V}_U^\top \mathbf{V}_1^\top \\ &= [V_1(y, 4) + V_1(y, 3)g_1] [V_1(x, 4) + V_1(x, 3)g_1] \lambda_{U,1}^j + [V_1(y, 4) + V_1(y, 3)g_2] [V_1(x, 4) + V_1(x, 3)g_2] \lambda_{U,2}^j \end{aligned} \quad (80)$$

Here we also have

$$\lambda_{U,2} > \lambda_{U,1} > 0 \quad (81)$$

since

$$u_1 + u_4 = h_1^2 + h_2^2 + h_3^2 + h_4^2 > 0 \quad (82)$$

and

$$\begin{aligned} \Delta - (u_1 + u_4)^2 &= -4u_1u_4 + 4u_2^2 \\ &= 4 \left[(h_1h_3 + h_2h_4)^2 - (h_1^2 + h_2^2)(h_3^2 + h_4^2) \right] \\ &= 4 \left[h_1^2h_3^2 + h_2^2h_4^2 + 2h_1h_2h_3h_4 - h_1^2h_3^2 - h_2^2h_3^2 - h_1^2h_4^2 - h_2^2h_4^2 \right] \\ &= -4(h_2h_3 - h_1h_4)^2 < 0 \end{aligned} \quad (83)$$

Therefore with increasing iteration numbers, the item multiplied by $\lambda_{U,1}^j$ gradually vanishes in the results. The limiting result of \mathcal{AB}^j turns out to be

$$\lim_{j \rightarrow +\infty} (\mathcal{AB})^j(x, y) = [V_1(y, 4) + V_1(y, 3)g_2] [V_1(x, 4) + V_1(x, 3)g_2] \lambda_{U,2}^j \quad (84)$$

And the quaternion solution is none about which column of \mathcal{AB}^j , and the result is the normalization of the following vector

$$\widehat{\mathbf{q}} = \begin{bmatrix} V_1(1, 4) + V_1(1, 3)g_2 \\ V_1(2, 4) + V_1(2, 3)g_2 \\ V_1(3, 4) + V_1(3, 3)g_2 \\ V_1(4, 4) + V_1(4, 3)g_2 \end{bmatrix} \quad (85)$$

123 3.3. Discussion of OLEQs

124 The three derived OLEQs can be used in different occasions. The OLEQ incorporates the weights
 125 so that the determination results are optimal in the sense of least square. When there is aid of gyroscope,
 126 the ROLEQ can achieve faster and more smooth estimates. The meaning of the proposed SOLEQ is
 127 that it owns very simple linear expression that may generate short and tidy analytic results for certain
 128 sensor combinations. Also, when required in application where the weights can hardly be accurately
 129 determined e.g. vision attitude determination, the SOLEQ could be an alternative choice, as well. The
 130 attitude determination results of the three OLEQs are evaluated in the following experimental section.

131 4. Simulations and Experiments

132 4.1. Simulation: Common Cases

In this sub-section, the sensor observations are simulated with random reference vectors and true DCM in

$$\mathbf{D}^b = \mathbf{C}_{true} \mathbf{D}^r + \varepsilon \quad (86)$$

where ε is the noise item which is supposed to be independent and subject to Gaussian distribution. The reference vectors and the standard deviations of noise items are selected according to the classical test samples by Markley (see Table 1), where the reference DCM \mathbf{C}_{true} is

$$\mathbf{C}_{true} = \begin{pmatrix} 0.352 & 0.864 & 0.360 \\ -0.864 & 0.152 & 0.480 \\ 0.360 & -0.480 & 0.800 \end{pmatrix} \quad (87)$$

Table 1. Test Cases

Case	Reference Vectors	Noise Standard Deviations
1	$\mathbf{D}_1^r = [1, 0, 0]^\top, \mathbf{D}_2^r = [0, 1, 0]^\top, \mathbf{D}_3^r = [0, 0, 1]^\top$	$\sigma_1 = 10^{-6}, \sigma_2 = 10^{-6}, \sigma_3 = 10^{-6}$
2	$\mathbf{D}_1^r = [1, 0, 0]^\top, \mathbf{D}_2^r = [0, 1, 0]^\top$	$\sigma_1 = 10^{-6}, \sigma_2 = 10^{-6}$
3	$\mathbf{D}_1^r = [1, 0, 0]^\top, \mathbf{D}_2^r = [0, 1, 0]^\top, \mathbf{D}_3^r = [0, 0, 1]^\top$	$\sigma_1 = 0.01, \sigma_2 = 0.01, \sigma_3 = 0.01$
4	$\mathbf{D}_1^r = [1, 0, 0]^\top, \mathbf{D}_2^r = [0, 1, 0]^\top$	$\sigma_1 = 0.01, \sigma_2 = 0.01$
5	$\mathbf{D}_1^r = [0.6, 0.8, 0]^\top, \mathbf{D}_2^r = [0.8, -0.6, 0]^\top$	$\sigma_1 = 10^{-6}, \sigma_2 = 0.01$
6	$\mathbf{D}_1^r = [1, 0, 0]^\top, \mathbf{D}_2^r = [1, 0.01, 0]^\top, \mathbf{D}_3^r = [1, 0, 0.01]^\top$	$\sigma_1 = 10^{-6}, \sigma_2 = 10^{-6}, \sigma_3 = 10^{-6}$
7	$\mathbf{D}_1^r = [1, 0, 0]^\top, \mathbf{D}_2^r = [1, 0.01, 0]^\top$	$\sigma_1 = 10^{-6}, \sigma_2 = 10^{-6}$
8	$\mathbf{D}_1^r = [1, 0, 0]^\top, \mathbf{D}_2^r = [1, 0.01, 0]^\top, \mathbf{D}_3^r = [1, 0, 0.01]^\top$	$\sigma_1 = 0.01, \sigma_2 = 0.01, \sigma_3 = 0.01$
9	$\mathbf{D}_1^r = [1, 0, 0]^\top, \mathbf{D}_2^r = [1, 0.01, 0]^\top$	$\sigma_1 = 0.01, \sigma_2 = 0.01$
10	$\mathbf{D}_1^r = [1, 0, 0]^\top, \mathbf{D}_2^r = [0.96, 0.28, 0]^\top, \mathbf{D}_3^r = [0.96, 0, 0.28]^\top$	$\sigma_1 = 10^{-6}, \sigma_2 = 0.01, \sigma_3 = 0.01$
11	$\mathbf{D}_1^r = [1, 0, 0]^\top, \mathbf{D}_2^r = [0.96, 0.28, 0]^\top$	$\sigma_1 = 10^{-6}, \sigma_2 = 0.01$
12	$\mathbf{D}_1^r = [1, 0, 0]^\top, \mathbf{D}_2^r = [0.96, 0.28, 0]^\top$	$\sigma_1 = 0.01, \sigma_2 = 10^{-6}$

133 Using the simulated samples, the mean attitude root mean-squared errors (RMSEs) in Euler angles
 134 are evaluated with our proposed algorithms OLEQ, SOLEQ and representative algorithms including
 135 QUEST and FLAE, which are shown in Table 2, 3, 4. Table 5 contains the computed average Wahba's
 136 loss function values by different cases and algorithms. These algorithms are executed on the MATLAB
 137 r2016 software on a PC for 10000 times with each data sample.

Table 2. Roll RMSE (deg)

Case	OLEQ	SOLEQ	QUEST	FLAE
1	4.3516×10^{-05}	6.1268×10^{-05}	4.3516×10^{-05}	4.3516×10^{-05}
2	5.9303×10^{-05}	6.0734×10^{-05}	5.9303×10^{-05}	5.9303×10^{-05}
3	4.3482×10^{-01}	6.0730×10^{-01}	4.3482×10^{-01}	4.3482×10^{-01}
4	6.0292×10^{-01}	6.1798×10^{-01}	6.0292×10^{-01}	6.0292×10^{-01}
5	4.3313×10^{-01}	4.3313×10^{-01}	4.9065×10^{-01}	$2.4281 \times 10^{+01}$
6	4.9590×10^{-03}	3.0793×10^{-01}	4.9590×10^{-03}	4.9590×10^{-03}
7	8.1132×10^{-03}	$1.3400 \times 10^{+00}$	8.1132×10^{-03}	8.1132×10^{-03}
8	$5.9553 \times 10^{+01}$	$6.2840 \times 10^{+01}$	$5.9553 \times 10^{+01}$	$5.9553 \times 10^{+01}$
9	$7.6662 \times 10^{+01}$	$7.6696 \times 10^{+01}$	$7.6662 \times 10^{+01}$	$7.6662 \times 10^{+01}$
10	$1.4313 \times 10^{+00}$	$1.7781 \times 10^{+00}$	$4.7663 \times 10^{+01}$	$1.5265 \times 10^{+00}$
11	$2.0254 \times 10^{+00}$	$2.0254 \times 10^{+00}$	$4.6392 \times 10^{+01}$	$2.8441 \times 10^{+00}$
12	$2.0818 \times 10^{+00}$	$2.0888 \times 10^{+00}$	$3.7218 \times 10^{+01}$	$1.7415 \times 10^{+01}$

Table 3. Pitch RMSE (deg)

Case	OLEQ	SOLEQ	QUEST	FLAE
1	4.0108×10^{-05}	5.7335×10^{-05}	4.0108×10^{-05}	4.0108×10^{-05}
2	5.2860×10^{-05}	5.6736×10^{-05}	5.2860×10^{-05}	5.2860×10^{-05}
3	4.0104×10^{-01}	5.6744×10^{-01}	4.0104×10^{-01}	4.0104×10^{-01}
4	5.3887×10^{-01}	5.7656×10^{-01}	5.3887×10^{-01}	5.3887×10^{-01}
5	3.9149×10^{-01}	3.9149×10^{-01}	4.4335×10^{-01}	$1.2561 \times 10^{+01}$
6	4.0121×10^{-05}	5.7809×10^{-05}	4.0121×10^{-05}	4.0121×10^{-05}
7	5.3398×10^{-05}	5.7657×10^{-05}	5.3398×10^{-05}	5.3398×10^{-05}
8	3.6755×10^{-01}	5.7326×10^{-01}	3.6755×10^{-01}	3.6755×10^{-01}
9	4.5938×10^{-01}	5.7880×10^{-01}	4.5938×10^{-01}	4.5938×10^{-01}
10	5.7186×10^{-05}	5.7186×10^{-05}	5.7184×10^{-05}	5.7186×10^{-05}
11	5.7845×10^{-05}	5.7845×10^{-05}	5.7846×10^{-05}	5.7844×10^{-05}
12	4.9161×10^{-01}	5.7554×10^{-01}	$7.9376 \times 10^{+00}$	$3.9359 \times 10^{+00}$

Table 4. Yaw RMSE (deg)

Case	OLEQ	SOLEQ	QUEST	FLAE
1	4.3587×10^{-05}	6.1084×10^{-05}	4.3587×10^{-05}	4.3587×10^{-05}
2	4.8694×10^{-05}	6.1015×10^{-05}	4.8694×10^{-05}	4.8694×10^{-05}
3	4.4127×10^{-01}	6.0868×10^{-01}	4.4127×10^{-01}	4.4127×10^{-01}
4	4.8593×10^{-01}	6.1289×10^{-01}	4.8593×10^{-01}	4.8593×10^{-01}
5	2.5186×10^{-01}	2.5186×10^{-01}	2.8536×10^{-01}	$1.7459 \times 10^{+01}$
6	3.6421×10^{-05}	6.1651×10^{-05}	3.6421×10^{-05}	3.6421×10^{-05}
7	4.8748×10^{-05}	6.0826×10^{-05}	4.8748×10^{-05}	4.8748×10^{-05}
8	3.9812×10^{-01}	6.1557×10^{-01}	3.9812×10^{-01}	3.9812×10^{-01}
9	4.9366×10^{-01}	6.1163×10^{-01}	4.9366×10^{-01}	4.9366×10^{-01}
10	6.1834×10^{-05}	6.1834×10^{-05}	6.1836×10^{-05}	6.1844×10^{-05}
11	6.2069×10^{-05}	6.2069×10^{-05}	6.2069×10^{-05}	6.2077×10^{-05}
12	3.1726×10^{-01}	6.1275×10^{-01}	$5.1968 \times 10^{+00}$	$2.8814 \times 10^{+00}$

Table 5. Loss Function Values

Case	OLEQ	SOLEQ	QUEST	FLAE
1	5.0651×10^{-13}	1.0130×10^{-12}	5.0651×10^{-13}	5.0651×10^{-13}
2	2.4901×10^{-13}	4.9802×10^{-13}	2.4901×10^{-13}	2.4901×10^{-13}
3	4.9338×10^{-05}	9.8666×10^{-05}	4.9338×10^{-05}	4.9338×10^{-05}
4	2.5369×10^{-05}	5.0736×10^{-05}	2.5369×10^{-05}	2.5369×10^{-05}
5	5.0582×10^{-13}	5.0582×10^{-13}	6.5095×10^{-13}	8.5878×10^{-10}
6	5.0422×10^{-13}	9.4333×10^{-10}	5.0422×10^{-13}	5.0422×10^{-13}
7	2.4728×10^{-13}	8.8239×10^{-09}	2.4728×10^{-13}	2.4728×10^{-13}
8	4.8216×10^{-05}	1.1593×10^{-04}	4.8216×10^{-05}	4.8216×10^{-05}
9	2.5327×10^{-05}	5.0651×10^{-05}	2.5327×10^{-05}	2.5327×10^{-05}
10	1.4827×10^{-12}	1.7575×10^{-12}	4.8431×10^{-10}	1.7195×10^{-12}
11	4.8573×10^{-13}	4.8573×10^{-13}	2.4106×10^{-10}	9.2333×10^{-13}
12	5.0105×10^{-13}	5.0105×10^{-05}	1.3143×10^{-10}	3.4336×10^{-11}

138 We first observe the attitude RMSEs. From the results of OLEQ, QUEST and FLAE, it is noticeable
139 to determine that they have the similar attitude determination accuracy. Combining the same statistics
140 in Table 5, the proposed OLEQ is well verified for its optimality. From the presented results, we see
141 that SOLEQ has larger attitude errors and loss function values other optimal methods. The proposed
142 SOLEQ is sub-optimal as it actually approximates the attitude estimator where the weights are ignored.

143 Therefore, this simulation scenario has validated the correctness and optimality of the proposed OLEQ
 144 and SOLEQ.

145 4.2. Simulation: Extreme Cases

$$\mathbf{D}_1^r = \begin{pmatrix} 1 \\ 0 \\ 0 \end{pmatrix}, \mathbf{D}_2^r = \begin{pmatrix} -0.99712 \\ 0.07584 \\ 0 \end{pmatrix}, \mathbf{D}_3^r = \begin{pmatrix} -0.99712 \\ -0.07584 \\ 0 \end{pmatrix} \quad (88)$$

$$\sigma_1 = 1 \text{ arcsec}, \sigma_2 = \sigma_3 = 1 \text{ deg}$$

146 Conventional Wahba's solutions face dilemma when exposed to some critical pairs of vector
 147 observations. For instance, Markley and Mortari give an example where the sensors are configured
 148 by (88) [40]. In such scenario, the root of the characteristic polynomial of the Davenport matrix can
 149 not be easily obtained by Newton iterations. The internal reason is given by Cheng [41] showing
 150 that it is resulted in by numerical loss according to the specific CPU word storage length. A flexible
 151 transformation of the characteristic polynomial is proposed then to significantly boost the convergence.
 152 As such configurations indeed happen in engineering practice, there is necessity to evaluate the
 153 proposed schemes by comparisons with representative solvers. With similar simulation techniques
 154 aforementioned, the vectors are simulated with given reference vectors and standard deviations by
 155 rotation of \mathbf{C}_{true} . Here the QUEST algorithm is revised to the Cheng's form. First, we mainly compare
 156 the two iterative methods QUEST and OLEQ because in our existing paper [25] the QUEST and
 157 FLAE have been proved to have very similar behaviour facing this extreme case. Here the iteration
 158 stops when the Euclidean norm of neighboring attitude quaternion difference is less than 1×10^{-8} .
 159 For QUEST, the maximum iteration number is set to 50. The obtained results are depicted in Fig.
 160 1. We can see that the supervised QUEST can obtain accurate quaternion solutions within several
 161 iterations. Actually, before the Cheng's improvement, the QUEST may exceed the maximum iteration
 162 number from time to time. The proposed OLEQ, however, shows better performance dealing with
 163 this extreme case. Also, the final mean loss function values of the two algorithms are computed as
 164 4.9890×10^{-11} and 2.8391×10^{-10} , which reveals that the proposed OLEQ can not only obtain faster
 165 solutions, but leads to smaller loss function values, compared with supervised QUEST. As is known to
 166 everyone, QUEST is the most representative Wahba's solution using Davenport's q-method. Many
 167 other algorithms like ESOQ, FOAM actually have the same performance with QUEST. Therefore, in
 168 this way, the OLEQ is proved to be faster and more robust than the whole class of the algorithms based
 169 on Davenport's q-method. This also shows that the presented novel attitude evolution method shows
 170 brand new abilities.

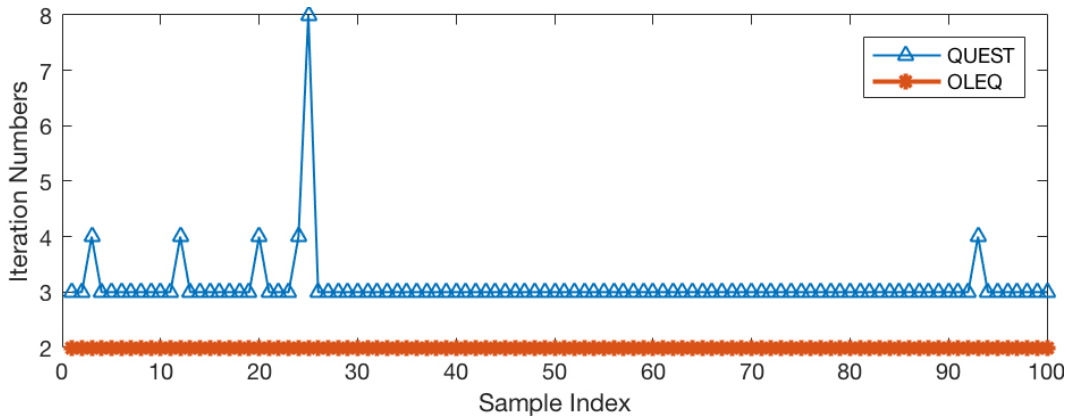


Figure 1. Iteration numbers of QUEST and OLEQ in face of an extreme case.

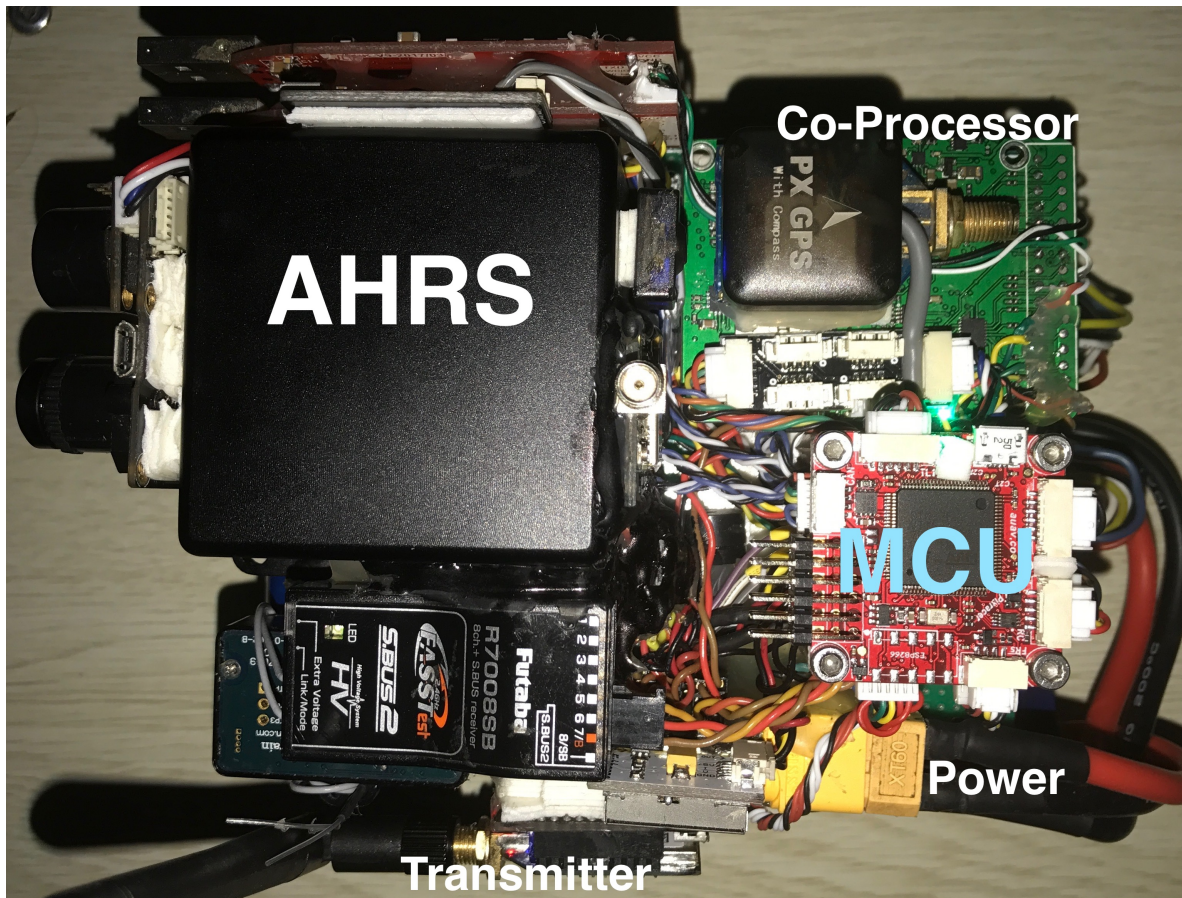


Figure 2. Designed hardware for algorithm implementation.

171 4.3. Experiment: Accelerometer-Magnetometer Case

172 In this sub-section, we conduct an experiment where the accelerometer-magnetometer
 173 combination is adopted. Such sensor combination is extensively applied in nowadays low-cost
 174 attitude estimation schemes. The accelerometer is pre-calibrated using the 6-face bias cancelling while
 175 the magnetometer is calibrated using the method proposed by Y. Wu et al. [42].

176 The hardware is constituted by a battery, a high-end attitude and heading reference system
 177 (AHRS) with high precision internal accelerometer, magnetometer and gyroscope, a transmitter for
 178 remote data transmission and a micro controller for implementation of the algorithm using C++
 179 language on the FreeRTOS. With the designed hardware platform shown in Fig. 2, we collect a data set
 180 with 10000 samplings.

181 The main purpose of this sub-section is to validate the performances of the proposed OLEQ,
 182 SOLEQ and ROLEQ since the AHRS has angular rate readouts. The compared results with the reference
 183 angles from representative methods are obtained (see Fig. 3, 4, 5). Note that here the weights between
 184 the accelerometer and magnetometer for Wahba's solution are chosen as 0.63 and 0.37 according to
 185 their respective noise characteristics. Yet, the local magnetometer's reference vector is calculated as
 186 $\mathbf{M}^r = (0.60311, 0, -0.79766)^\top$ in Wuxi, Jiangsu Province, China.

187 In Fig. 3, the reference angles, QUEST solutions and SOLEQ solutions have been presented. The
 188 results indicate that the proposed sub-optimal estimator can estimate the attitude angles with similar
 189 macroscopic accuracy. Detailed attitude errors are plotted in Fig. 4 and 5. We may notice that in
 190 general, these algorithms have the same errors with respect to reference. The second picture shows
 191 that the overall attitude accuracy of the ROLEQ is slightly smaller than the others. This is because it is
 192 first processed by the angular rate data, which can be equivalent to a smoothing procedure.

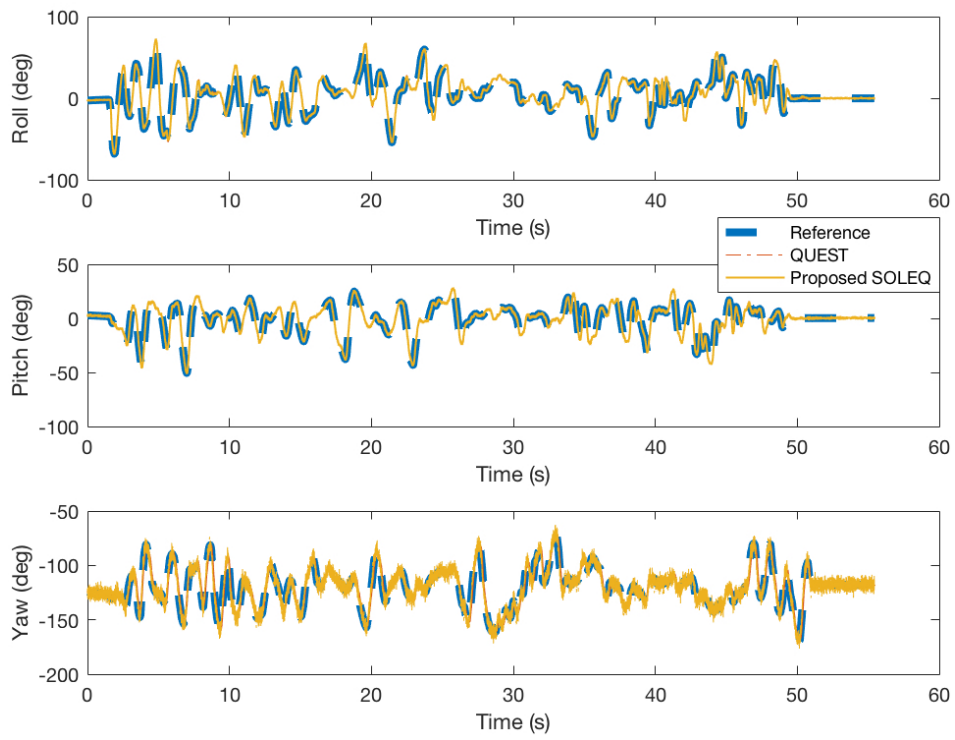


Figure 3. Experiment results using QUEST and SOLEQ.

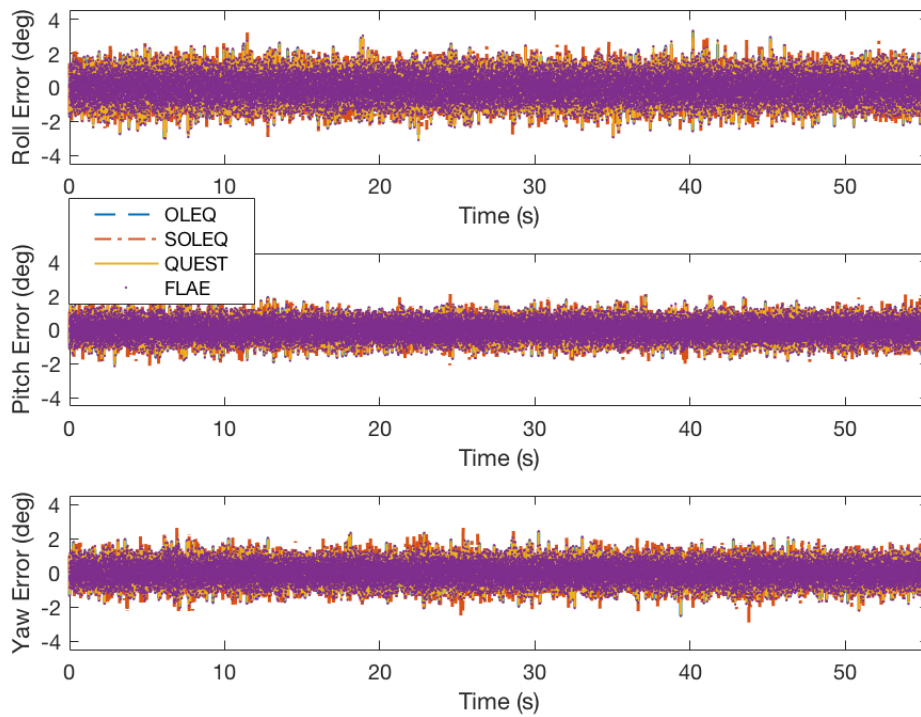


Figure 4. Experiment results of OLEQ, SOLEQ and representative algorithms using sampled data and different algorithms.

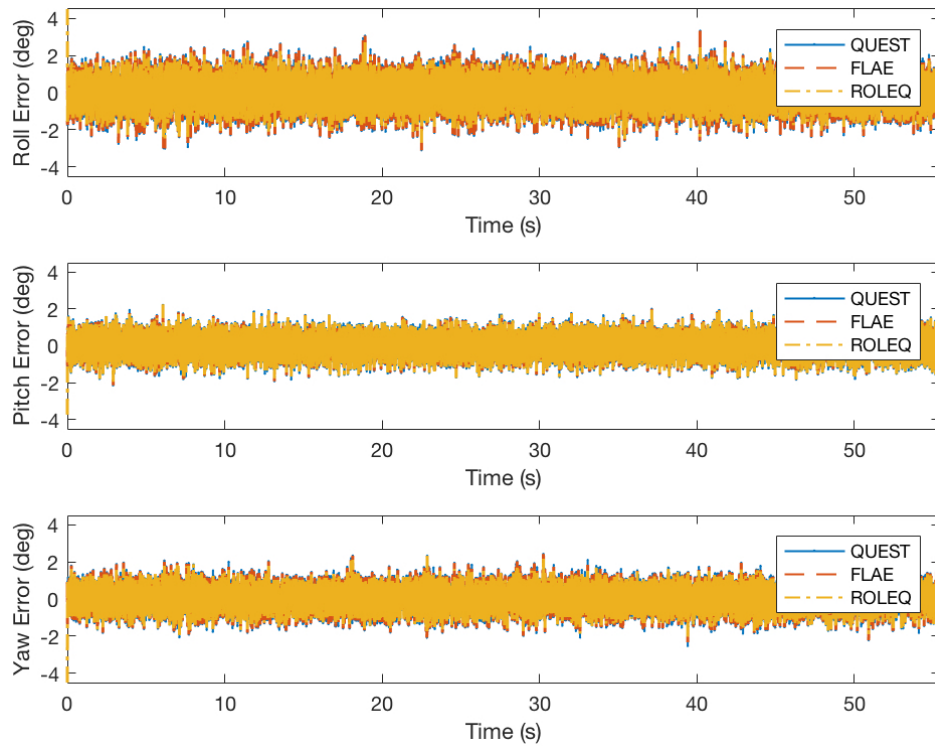


Figure 5. Experiment results of ROLEQ and representative algorithms using sampled data and different algorithms.

193 4.4. Experiment: GNSS Attitude Determination for Land Vehicles

194 The GNSS receiver is widely employed in the attitude determination tasks for land and unmanned
 195 aerial vehicles. In this experiment, we use a designed rover (see Fig. 6) to validate the feasibility of the
 196 proposed algorithm for GNSS attitude determination.



Figure 6. The designed multi-functional rover for validation of proposed algorithms.

197 The rover is armed with the aforementioned navigation computer and employs an external
 198 ublox M8N GPS module with serial comm connection to the board at the sampling frequency of
 199 5Hz. This rover is controlled by a handheld 2.4GHz transmitter and the onboard Pixhawk autopilot
 200 generates PID controlling commands to the servos and motors according to internal measurements.
 201 In this experiment, the rover is ran on a playground of UESTC and we pick up one period of data
 202 in which the GPS velocity is valid. In the data history, the magnetometer was distorted by outer
 203 unknown electromagnetic and ferromagnetic fields. Also, during the execution process, sensor raw
 204 measurements from gyroscope, accelerometer are also logged with the speed of 250Hz. The raw data
 205 is shown in Fig. 7.

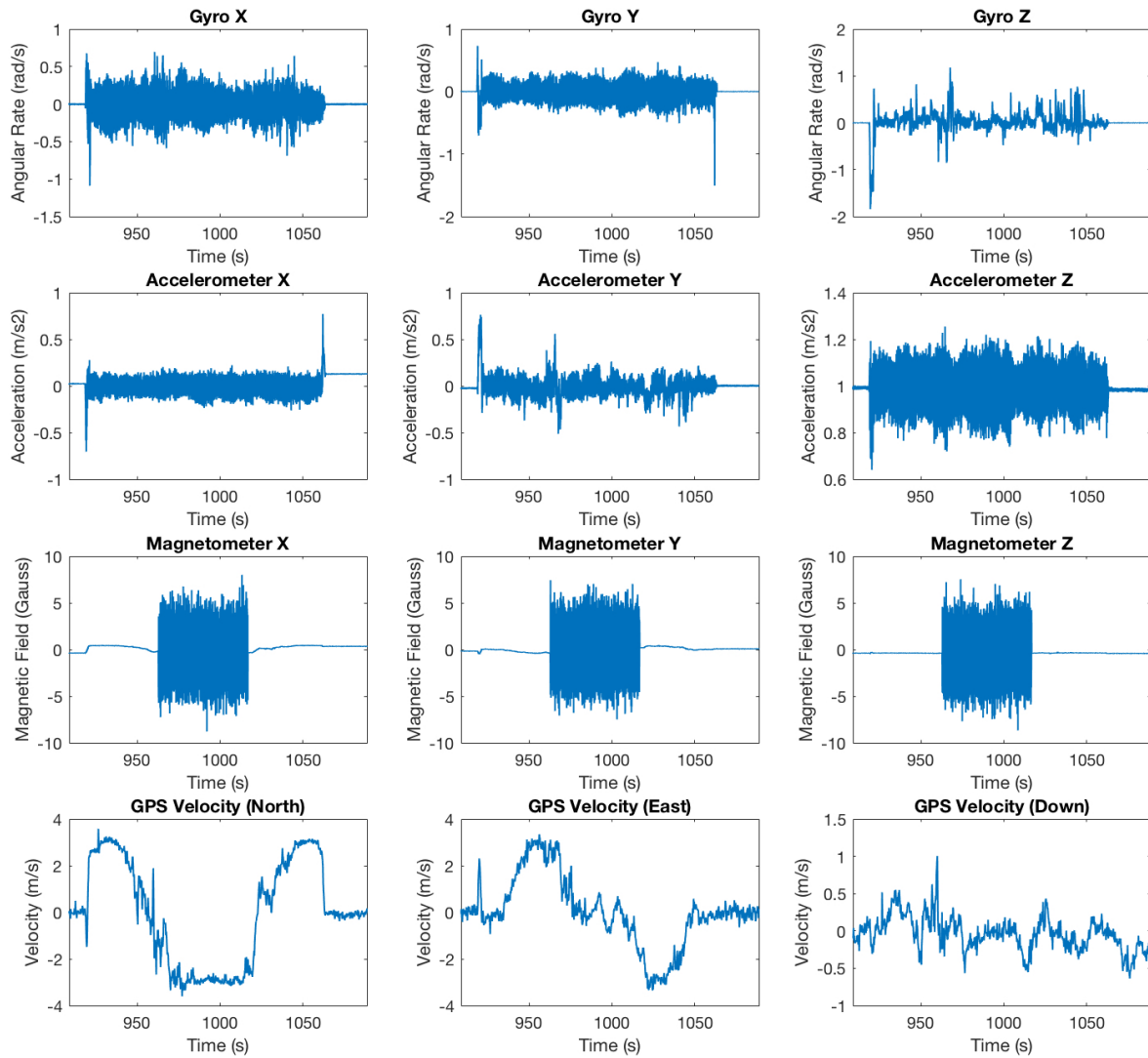


Figure 7. Raw sensor measurements from the logging memory.

206 According to the sensor noise characteristics, the weights of the accelerometer-magnetometer
 207 combination are given by 0.9 and 0.1 respectively. While for the accelerometer-magnetometer-GNSS
 208 one, the weights are chosen as 0.474, 0.05, 0.474 respectively. The reference vector of magnetometer is
 209 determined by the initial GPS position with the IGRF model. By making use of algorithms including
 210 QUEST, FLAE, OLEQ and SOLEQ, the computation results are summarized in Fig. 8 and 9.

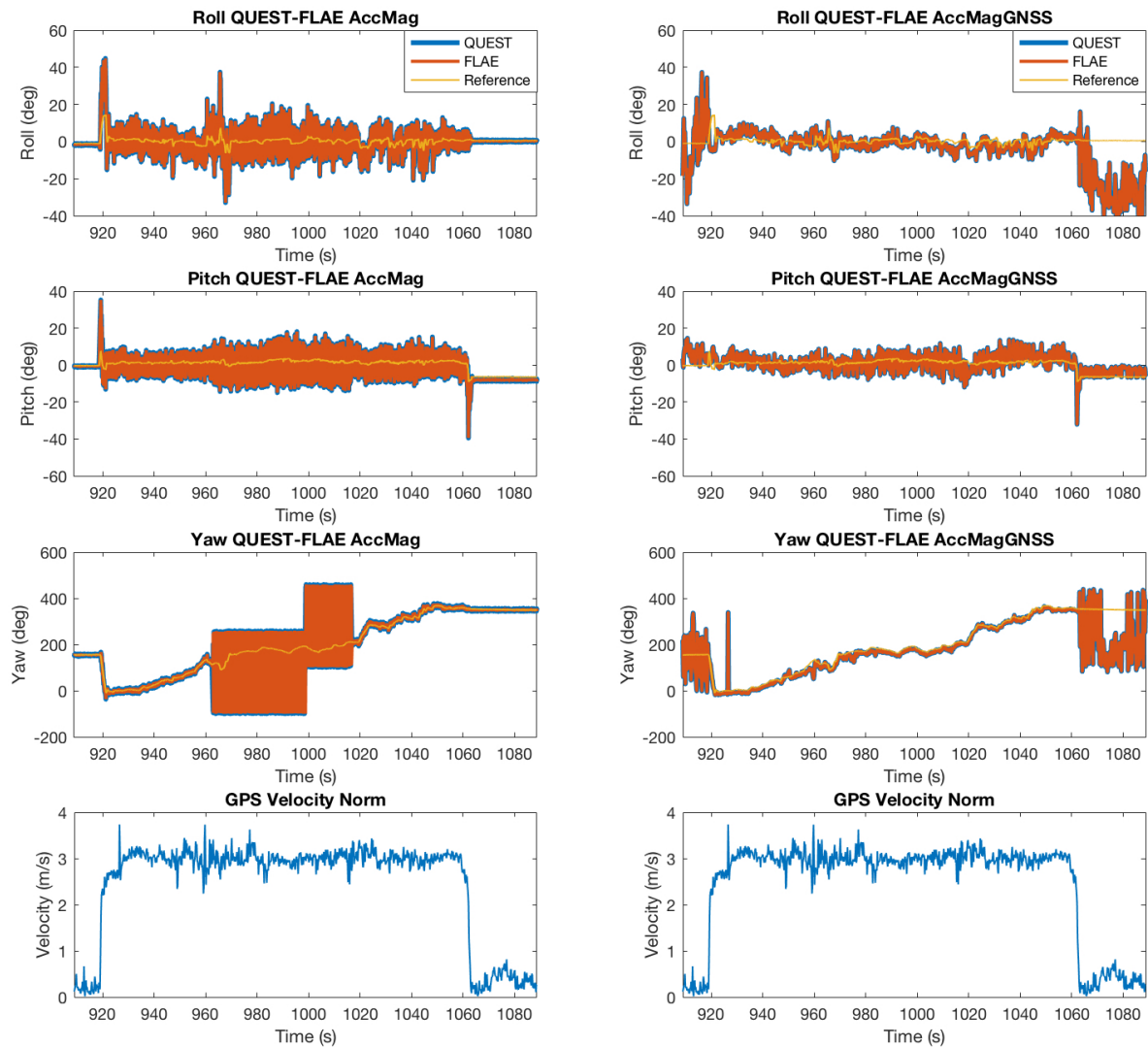


Figure 8. Attitude determination from accelerometer, magnetometer and velocity output of GNSS receiver, by means of QUEST and FLAE.

211 We especially add the GPS velocity norm under Euler angle results to illustrate the influence of the
 212 velocity scalar to the attitude determination results. In principle, when the vehicle is not moving with
 213 relative discriminative velocities, the GPS receiver can not give accurate speed estimates. Therefore, it
 214 is shown in the initial stage of the attitude determination results where GNSS takes part in that the
 215 determination accuracy of the yaw angle is seemingly very poor. As the velocity increases, the accuracy
 216 is improved very fast accordingly. The accelerometer-magnetometer combination is largely distorted
 217 by the magnetic disturbances. The integrated results of roll, pitch and more over, the yaw angles are
 218 influenced generating very obvious differences with reference angles. With the aid of GNSS velocity,
 219 the corresponding attitude determination accuracy is not damaged because the Wahba's solution
 220 balances the sensor inputs by the weights. It is observed that the OLEQ is validated to have almost
 221 the same accuracy for normal sensors in aforementioned section and in this section such behaviour
 222 holds as well. The SOLEQ, however, does not employ the weights and therefore produces relative
 223 bad estimates but for GNSS case, it is still better than accelerometer-magnetometer ones. The results
 224 provided us with the information of the validity of the proposed algorithms especially the OLEQ.

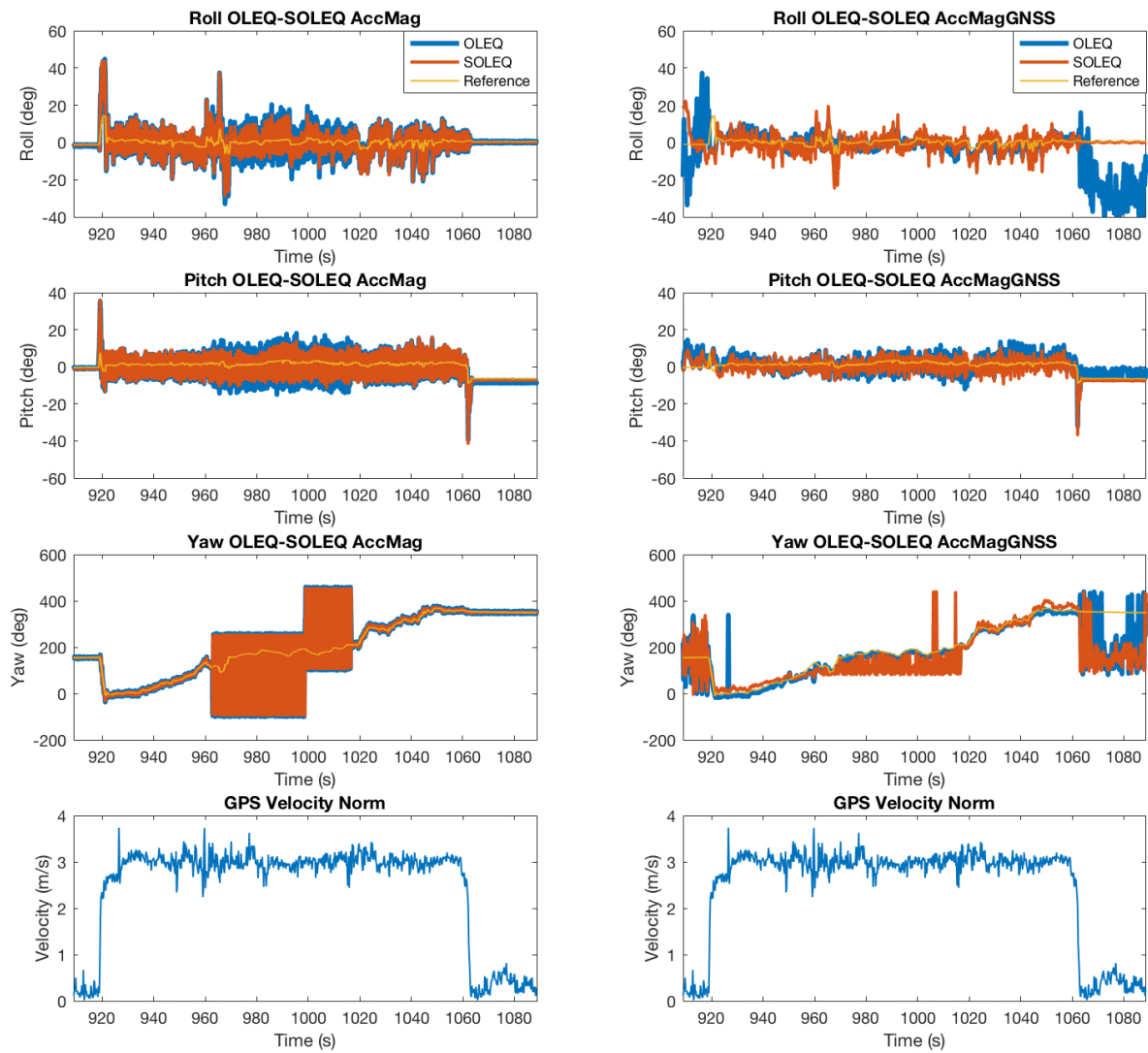


Figure 9. Attitude determination from accelerometer, magnetometer and velocity output of GNSS receiver, by means of OLEQ and SOLEQ.

225 4.5. Computation Time

226 From another point of view, the time consumption of various algorithms should be investigated.
 227 The time consumption is calculated on the embedded platform by C++ programming language that
 228 ensures the fairness. A rough evaluation is done with two pairs of vector observations in few samples
 229 which shows direct time consumption results (see Fig. 10). As shown in the figure, for two pairs of
 230 vector observations, the three proposed algorithms' computation times are between QUEST and FLAE.
 231 However, from the expressions of the algorithms presented before, the number of vector observations
 232 is influential to the final time consumption. Hence with the simulation samples, each algorithm is
 233 again tested for 20000 times with different vector observation numbers. The time consumption is
 234 averaged, which is plotted in Fig. 11. The results show that the algorithms are all linear owing
 235 the time complexities of $O(n)$. QUEST, OLEQ and ROLEQ join at the vector observation number of
 236 20. For common tasks, such number covers most sensor amounts. Although FLAE owns the least
 237 time consumption, it can not overcome drawbacks of extreme cases so well as OLEQ. That is to
 238 say, the proposed algorithms can replace the original algorithms for faster and more robust attitude
 239 determination.

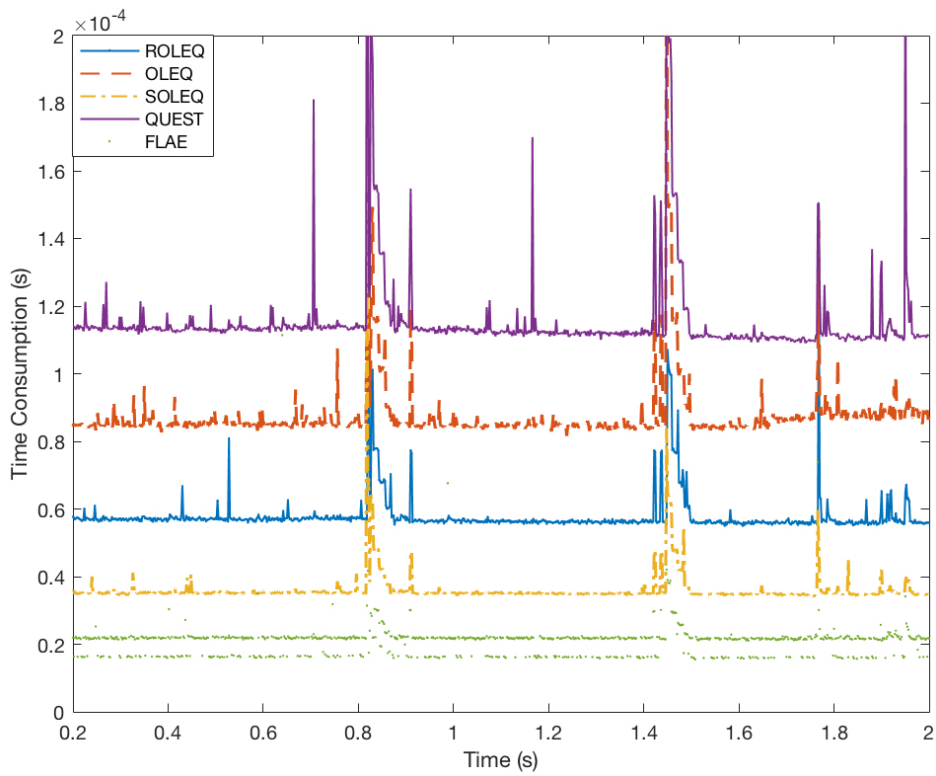


Figure 10. Time consumption of various algorithms.

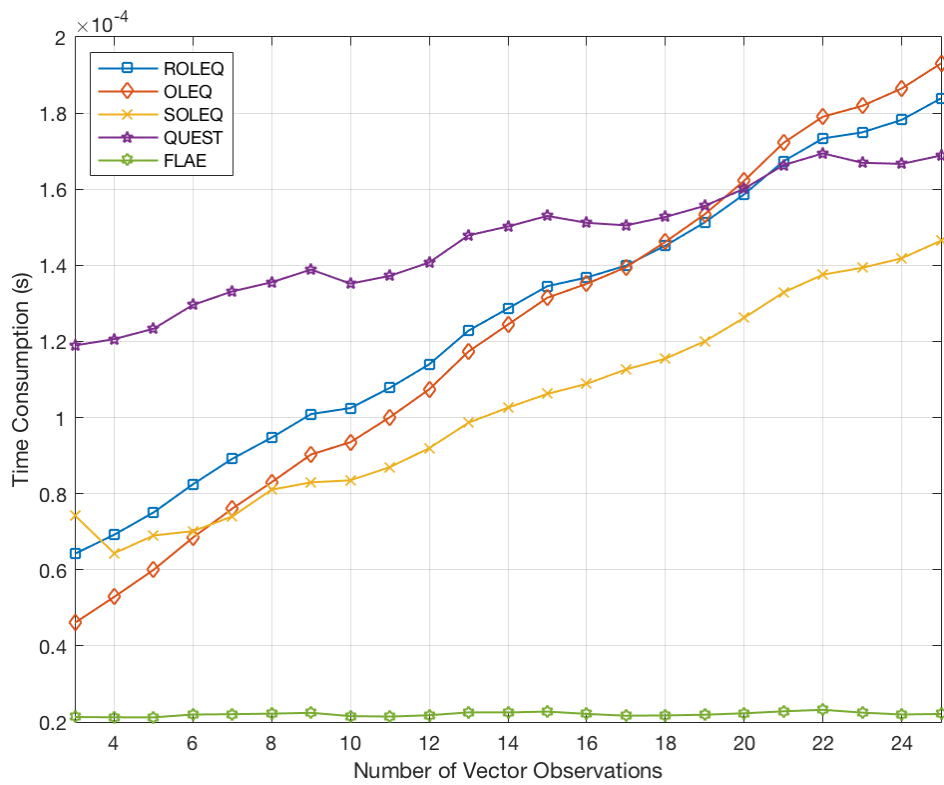


Figure 11. Time consumption of algorithms with respect to numbers of vector observations.

5. Conclusion

This paper revisits the attitude determination from vector observation for a GNSS/AM case study. Novel linear algorithms are designed to obtain accurate attitude estimates in the sense of least-square. Handling in this manner, the computed quaternion is identical or suboptimal with respect to conventional Wahba's solutions including QUEST and FLAE. Numerical simulations exhibit that the proposed OLEQs own the similar accuracy with representative solvers. It is also evaluated that facing extreme cases, the OLEQs show much more robustness less computation iterations. The computation speeds of OLEQs are tested revealing that they belong to computationally efficient algorithms. Moreover, a real vehicular experiment of GNSS/AM system is designed and conducted showing the effectiveness of the proposed OLEQs in real-world embedded applications. The presented approach provides the audience with a brand new viewpoint of attitude evolution and hopefully would benefit related multi-sensor attitude determination applications.

Acknowledgments: This research is supported by National Natural Science Foundation of China under the grant number of 41604025. Dr. F. L. Markley provided constructive suggestions on the internal theory of this paper. Yunheng Inc., Chengdu gave us the instrumentation services during experimental validation. We genuinely thank them for their support.

Conflicts of Interest: The authors declare no conflict of interests regarding the publication of this paper.

1. Zhou, Z.; Li, Y.; Liu, J.; Li, G. Equality constrained robust measurement fusion for adaptive kalman-filter-based heterogeneous multi-sensor navigation. *IEEE Transactions on Aerospace and Electronic Systems* **2013**, *49*, 2146–2157.
2. Zhou, Z.; Li, Y.; Zhang, J.; Rizos, C. Integrated Navigation System for a Low-Cost Quadrotor Aerial Vehicle in the Presence of Rotor Influences. *Journal of Surveying Engineering* **2017**, *143*, 05016006.
3. Chang, G.; Xu, T.; Wang, Q. M-estimator for the 3D symmetric Helmert coordinate transformation. *Journal of Geodesy* **2017**.
4. Wu, Y.; Wang, J.; Hu, D. A New Technique for INS / GNSS Attitude and Parameter Estimation Using Online Optimization. *IEEE Transactions on Signal Processing* **2014**, *62*, 2642–2655.
5. Chang, L.; Qin, F.; Zha, F. Pseudo Open-Loop Unscented Quaternion Estimator for Attitude Estimation. *IEEE Sensors Journal* **2016**, *16*, 4460–4469.
6. Han, S.; Wang, J. Quantization and colored noises error modeling for inertial sensors for GPS/INS integration. *IEEE Sensors Journal* **2011**, *11*, 1493–1503.
7. Chang, L.; Li, J.; Chen, S. Initial Alignment by Attitude Estimation for Strapdown Inertial Navigation Systems. *IEEE Transactions on Instrumentation and Measurement* **2015**, *64*, 784–794.
8. Marins, J.; Yun, X.; Bachmann, E.; McGhee, R.; Zyda, M. An extended Kalman filter for quaternion-based orientation estimation using MARG sensors. *Proceedings 2001 IEEE/RSJ International Conference on Intelligent Robots and Systems. Expanding the Societal Role of Robotics in the the Next Millennium (Cat. No.01CH37180)* **2001**, *4*.
9. Tian, Y.; Wei, H.; Tan, J. An adaptive-gain complementary filter for real-time human motion tracking with MARG sensors in free-living environments. *IEEE Transactions on Neural Systems and Rehabilitation Engineering* **2013**, *21*, 254–264.
10. Aleshechkin, A. Algorithm of GNSS-based attitude determination. *Gyroscopy and Navigation* **2011**, *2*, 269.
11. Grewal, M.; Andrews, A. Kalman filtering: theory and practice using MATLAB, 2001.
12. Niu, X.; Nassar, S.; EL-SHEIMY, N. An Accurate Land-Vehicle MEMS IMU/GPS Navigation System Using 3D Auxiliary Velocity Updates. *Navigation* **2007**, *54*, 177–188.
13. Niu, X.; Nasser, S.; Goodall, C.; El-Sheimy, N. A universal approach for processing any MEMS inertial sensor configuration for land-vehicle navigation. *The Journal of Navigation* **2007**, *60*, 233–245.
14. Gebre-Egziabher, D.; Elkaim, G.H. MAV attitude determination by vector matching. *IEEE Transactions on Aerospace and Electronic Systems* **2008**, *44*.
15. Zhang, J.; Zhang, K.; Grenfell, R.; Deakin, R. Short note: On the relativistic Doppler effect for precise velocity determination using GPS. *Journal of Geodesy* **2006**, *80*, 104–110.

- 290 16. Zhou, Z.; Li, B. Optimal Doppler-aided smoothing strategy for GNSS navigation. *GPS solutions* **2017**,
291 21, 197–210.
- 292 17. Geng, J.; Bock, Y.; Melgar, D.; Crowell, B.W.; Haase, J.S. A new seismogeodetic approach applied to GPS
293 and accelerometer observations of the 2012 Brawley seismic swarm: Implications for earthquake early
294 warning. *Geochemistry, Geophysics, Geosystems* **2013**, *14*, 2124–2142.
- 295 18. Geng, J.; Melgar, D.; Bock, Y.; Pantoli, E.; Restrepo, J. Recovering coseismic point ground tilts from
296 collocated high-rate GPS and accelerometers. *Geophysical Research Letters* **2013**, *40*, 5095–5100.
- 297 19. Wahba, G. A Least Squares Estimate of Satellite Attitude, 1965.
- 298 20. Shuster, M.D.; Oh, S.D. Three-axis attitude determination from vector observations. *Journal of Guidance,
299 Control, and Dynamics* **1981**, *4*, 70–77.
- 300 21. Markley, F.L. Attitude Determination using Vector Observations and the Singular Value Decomposition,
301 1988.
- 302 22. Mortari, D. ESOQ: A Closed-Form Solution to the Wahba Problem. *The Journal of the Astronautical Sciences*
303 **1997**, *45*, 195–204.
- 304 23. Davenport, P.B. A vector approach to the algebra of rotations with applications. Technical Report August,
305 1968.
- 306 24. Chang, G.; Xu, T.; Wang, Q. Error analysis of Davenport’s q method. *Automatica* **2017**, *75*, 217–220.
- 307 25. Wu, J.; Zhou, Z.; Li, R.; Yang, L. Attitude Determination Using a Single Sensor Observation: Analytic
308 Quaternion Solutions and Property Discussion. *IET Science, Measurement & Technology (Accepted)* **2017**.
- 309 26. Yang, Y.; Zhou, Z. An analytic solution to Wahbas problem. *Aerospace Science and Technology* **2013**, *30*, 46–49,
310 [1309.5679].
- 311 27. Yang, Y. Attitude determination using Newton’s method on Riemannian manifold. *Proceedings of the
312 Institution of Mechanical Engineers, Part G: Journal of Aerospace Engineering* **2015**, *0*, 1–6.
- 313 28. Forbes, J.R.; de Ruiter, A.H.J. Linear-Matrix-Inequality-Based Solution to Wahba’s Problem. *Journal of
314 Guidance, Control, and Dynamics* **2015**, *38*, 147–151.
- 315 29. Mahony, R.; Hamel, T.; Pflimlin, J.M. Nonlinear complementary filters on the special orthogonal group.
316 *IEEE Transactions on Automatic Control* **2008**, *53*, 1203–1218.
- 317 30. Madgwick, S.O.H.; Harrison, A.J.L.; Vaidyanathan, R. Estimation of IMU and MARG orientation using a
318 gradient descent algorithm. *IEEE International Conference on Rehabilitation Robotics* **2011**.
- 319 31. Arun, K.S.; Huang, T.S.; Blostein, S.D. Least-Squares Fitting of Two 3-D Point Sets. *IEEE Transactions on
320 Pattern Analysis and Machine Intelligence* **1987**, *PAMI-9*, 698–700.
- 321 32. Ye, C.; Hong, S.; Tamjidi, A. 6-DOF Pose Estimation of a Robotic Navigation Aid by Tracking Visual and
322 Geometric Features. *IEEE Transactions on Automation Science and Engineering* **2015**, *12*, 1169–1180.
- 323 33. Markley, F.L.; Mortari, D. Quaternion attitude estimation using vector observations. *Journal of the
324 Astronautical Sciences* **2000**, *48*, 359–380.
- 325 34. Markley, F.L.; Mortari, D. How to estimate attitude from vector observations. *Advances in the Astronautical
326 Sciences* **2000**, *103*, 1979–1996.
- 327 35. Markley, F.L. Humble problems. *Advances in the Astronautical Sciences* **2006**, *124 II*, 2205–2222.
- 328 36. Wu, J.; Zhou, Z.; Chen, J.; Fourati, H.; Li, R. Fast Complementary Filter for Attitude Estimation Using
329 Low-Cost MARG Sensors. *IEEE Sensors Journal* **2016**, *16*, 6997–7007.
- 330 37. Shuster, M.D. Filter QUEST or REQUEST. *Journal of Guidance, Control, and Dynamics* **2009**, *32*, 643–645.
- 331 38. Horn, R.A.; Johnson, C.R. *Matrix analysis*; Cambridge university press, 2012.
- 332 39. Yang, Y. Spacecraft attitude determination and control: Quaternion based method. *Annual Reviews in
333 Control* **2012**, *36*, 198–219.
- 334 40. Markley, F.L.; Mortari, D. Quaternion Attitude Estimation Using Vector Observations. *Journal of the
335 Astronautical Sciences* **2000**, *48*, 359–380.
- 336 41. Cheng, Y.; Shuster, M.D. Improvement to the Implementation of the QUEST Algorithm. *Journal of Guidance,
337 Control, and Dynamics* **2014**, *37*, 301–305.
- 338 42. Wu, Y.; Shi, W. On Calibration of Three-Axis Magnetometer. *IEEE Sensors Journal* **2015**, *15*, 6424–6431.